

Eighth Quarterly Progress Report

June 26 through September 26, 1985

NIH Contract N01-NS-2356

Speech Processors for Auditory Prostheses

Prepared by

Blake S. Wilson, Charles C. Finley and Dewey T. Lawson

Neuroscience Program Office
Research Triangle Institute
Research Triangle Park, NC 27709

CONTENTS

I. Introduction	3
II. Ensemble Models	5
A. <u>Construction of a simple ensemble model</u>	8
B. <u>Effects of pulse parameters on neural response fields</u>	17
C. <u>Manipulation of latency profiles to code stimulus intensity</u>	20
D. <u>Manipulation of latency profiles to code stimulus frequency</u>	23
E. <u>Illustration of temporal channel interactions</u>	28
F. <u>Effects of a heterogeneous neural population on response fields elicited by bipolar and monopolar stimulation</u>	31
G. <u>Remarks on dendritic versus axonal stimulation</u>	48
H. <u>Concluding remarks</u>	51
III. Plans for the Next Quarter	54
IV. Acknowledgement	55
V. References	56
<u>Appendix 1: Abstracts Prepared in the Present Quarter</u>	60

I. Introduction

The purpose of this project is to design and evaluate speech processors for auditory prostheses. Ideally, the processors will extract (or preserve) from speech those parameters that are essential for intelligibility and then appropriately encode these parameters for electrical stimulation of the auditory nerve. Work in the present quarter included the following:

1. Further development of hardware and software for tests with our next patient, to be implanted at the Duke University Medical Center on 10/24/85;
2. Completion of the laboratory at Duke for these tests;
3. Initial development of hardware/software links to synchronize the outputs of our computer-simulated speech processors to the video displays of lipreading tests (developed at the University of Iowa and at Stanford University), for use in comparative measurements of speech recognition with lipreading alone, lipreading plus speech processor, and speech processor alone;
4. Preparation for our annual presentation at the Neural Prosthesis Workshop and for three additional presentations at the 38th ACEMB and 8th IEEE-EMBS Meetings; and
5. Continued development of ensemble models of the spatial and temporal patterns of neural discharge produced by intracochlear electrical stimulation.

In this report we will present initial results from the simplest of our ensemble models (point 5 above). These results suggest, in part, that control of the fine temporal structure of discharges in the electrically-evoked neural volley may provide improved coding of fundamental attributes of the auditory stimulus such as frequency and intensity. In addition, the model illustrates effects of (a) manipulation of pulse parameters on neural response fields; (b) simultaneous stimulation of adjacent channels in a

multichannel electrode array; and (c) a heterogeneous neural population on response fields elicited by bipolar and monopolar stimulation. Finally, model results suggest ways in which good performance might be obtained in certain "star" patients with single-channel devices or with multichannel devices using monopolar electrodes.

Further description of the activities indicated in points 1 and 3 above is deferred for now, but will be presented in future reports.

II. Ensemble Models

In the following sections we will describe models that predict the spatial and temporal patterns of neural responses produced by intracochlear electrical stimulation. All of the "ensemble models" to be presented actually consist of two models: one to describe the field patterns generated by intracochlear electrodes and the other to describe the neural responses evoked by the imposed electric fields. Table 1 lists these elements for three ensemble models in an order of increasing model complexity. The simplest ensemble model couples an exponential-falloff model of field patterns with a mathematical description of strength-duration curves for intracochlear electrical stimulation. This combined model (ensemble model 1) provides a powerful tool for demonstrating basic patterns of neural responses evoked by a wide range of electrodes and stimuli. In addition, it stands on a firm foundation of previous work in which the exponential-falloff model was used (see, e.g., Black and Clark, 1980; Merzenich and White, 1977; O'Leary *et al.*, 1985) and in which measurements of strength-duration relationships were made for various configurations of intracochlear electrodes (Loeb *et al.*, 1983; van den Honert and Stypulkowski, 1984). Ensemble model 1 is therefore broadly applicable to different electrode arrays and can provide an overall picture of neural response fields without invoking a long list of assumptions. However, comparison of results produced by model 1 and preliminary versions of the more-complex models listed in Table 1 demonstrates that model 1 does not predict potentially-important details of the response fields, at least for some conditions of stimulation with the UCSF electrode array. The primary deficits of model 1 are that (1) the field model does not describe the complex voltage profiles likely to be imposed along dendrites and axons for spatially-selective electrode arrays and (2) the neural model assumes that the amplitude of the electric field at a single point is the excitatory aspect of stimulation when, in fact, both voltage gradients and amplitudes acting at different locations along cochlear neurons probably contribute to excitation. Finally, ensemble model 1 is limited in that it can account only for the first neural volley to a transient stimulus; it cannot predict the temporal patterns of responses to steady-state stimuli such as sinusoids, or to repetitive transient stimuli for repetition periods much below 10 msec.

Table 1. Elements of Ensemble Models.

ensemble	<u>model</u>	<u>field model element</u>	<u>neural model element</u>
1		exponential falloffs	strength-duration curves
2		finite-difference, two-dimensional model of fields produced by the UCSF array, in which voltage profiles along along neurons are estimated by coupling spiral-plane results with transverse-plane results	modified McNeal model, in which the Frankenhauser-Huxley equations are used to describe node dynamics and in which membrane parameters appropriate for auditory nerve fibers are substituted for the original parameters of much-larger, uniform-diameter fibers
3		finite-element, three-dimensional model of fields produced within the entire cochlear volume by various electrode arrays, including the UCSF electrode array	extension of McNeal model, in which the finite impedances of myelin segments are represented and in which the node dynamics are altered to reflect those of mammalian fibers

The next two levels of ensemble models listed in Table 1 address some of the deficiencies and limitations just mentioned for ensemble model 1. In particular, ensemble model 2 is designed to provide a closer approximation to events that probably occur in ears implanted with the UCSF electrode array. Voltage profiles along peripheral dendrites and central axons are estimated by coupling results from our finite-difference, spiral-plane model of field patterns (see QPR 5) with results from our transverse-plane model of field patterns (see QPR 2). The voltage profiles thus derived are then

applied to the exterior of a modified McNeal model of myelinated nerve fibers (McNeal, 1976). In this model the Frankenhauser-Huxley equations are used to describe the nonlinear dynamics of the nodes (for frog, at 20° C), and passive properties of the nodes and node-to-node axoplasmic resistance are derived from measurements of axon diameter and nodal length. Substitution of such measurements from auditory nerve fibers (from cat, see Liberman and Oliver, 1984) provides a first approximation to nodal membrane capacitance and resistance, and to internodal resistance, at dendritic and axonal sites. Ensemble model 2 is therefore likely to be useful for determining the probable sites of nodes to first enter regenerative states with different stimulus waveforms and levels of excitation. However, this ensemble model, like ensemble model 1, cannot be used to predict the temporal dynamics of neural responses beyond the initial, "first-pop" response.

Ensemble model 3 is the most general of the listed models in that it is designed to simulate (a) the electric field patterns produced by arbitrary placements of electrodes in the complex, heterogeneous structure of the cochlea and (b) the propagation of action potentials and temporal dynamics of responses of neurons whose node and refractory characteristics approximate those of mammalian fibers at 37° C. The field model includes a full three-dimensional, finite-element representation of isotropic (e.g., perilymph) and anisotropic (e.g., auditory nerve and bone) impedances in the ear. Impedance data are obtained by digitizing structural outlines from transverse sections of the cochlea with a digitizer pad, and then assigning known or estimated impedances to the outlined structures. Because many impedances can only be estimated from measurements of similar structures elsewhere in the body (e.g., bone), algorithms for sensitivity analyses are built into the model so that each assumption can be examined for its potential impact on the final results.

The neural model element of ensemble model 3 is a further extension of the McNeal model, in which the finite impedances of myelin segments are represented and in which the node dynamics are altered to reflect those of mammalian fibers. This extension allows for computation of neural responses other than simple prethreshold responses, enables observation of propagation of spike activity, and permits the study of responses to complex, arbitrary stimuli over time (see QPR 4, section III). Like the field model, though, many parameters of the extended neural model can only be roughly

approximated. Sensitivity analyses and directed in vivo confirmations of model predictions are therefore essential for meaningful interpretation of the results. Such in vivo studies are planned and algorithms for sensitivity analyses are built into the neural model.

As indicated in the previous paragraphs, each of the three ensemble models has its advantages and disadvantages. These advantages and disadvantages are summarized in Table 2. In general, model complexity and number of assumptions increase with model number. To illustrate applications of ensemble models, we will review in the next sections results obtained from ensemble model 1. As we will show, these results are useful for visualizing the general shapes of response fields produced by intracochlear electrical stimulation and for conducting "thought experiments" on underlying mechanisms of perception with cochlear implants. Elucidation of details in the response fields, and of long-term temporal patterns of neural discharge, requires application of the more-complex models listed in Table 1. Results from these models will be presented in future quarterly reports.

A. Construction of a simple ensemble model

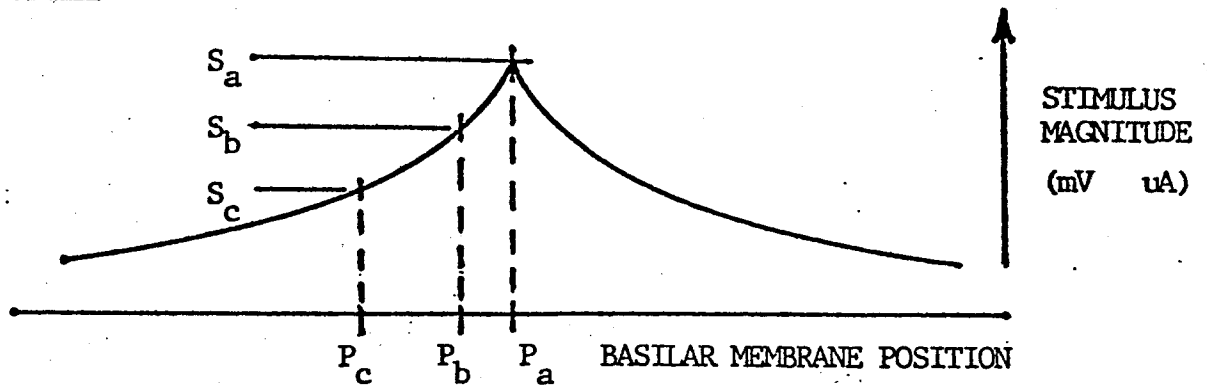
As mentioned above, the simplest of our ensemble models couples an exponential-falloff model of field patterns with a mathematical description of strength-duration curves for intracochlear electrical stimulation. A basic outline of this combined model is presented in Fig. 1. First, in the top panel the magnitude of the electric field is plotted as a function of distance along the cochlear partition. The peak of the field pattern corresponds to the position of the stimulating electrode or pair of electrodes, and is labeled P_a on the diagram. The stimulus level at the peak is labeled S_a , and locations and stimulus levels away from the peak are labeled P_b , S_b and P_c , S_c .

In the middle panel of Fig. 1 the effects of the stimulus field on individual neurons are illustrated. Each neuron is described by a simple strength-duration curve, which specifies the minimum duration of a pulse required to elicit a neural response for a given stimulus intensity. For the stimulus field shown, neuron A is excited at time t_a , neuron B at time

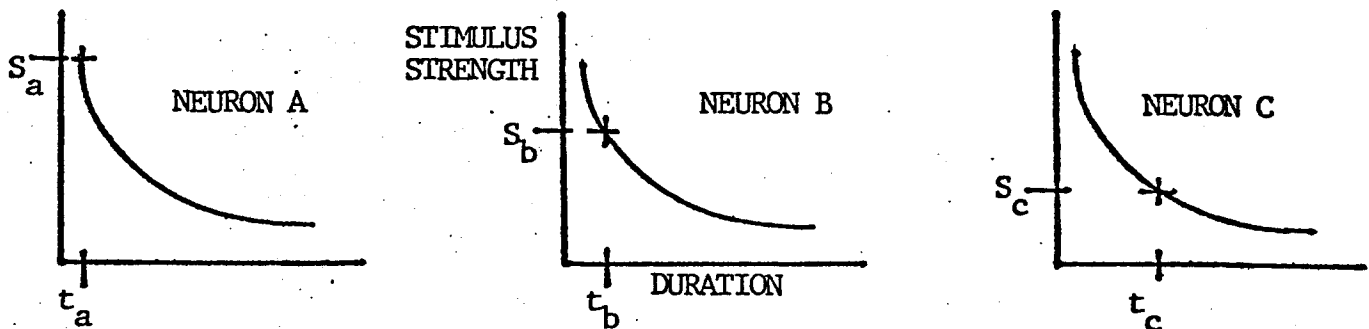
Table 2. Advantages and Disadvantages of the Ensemble Models Listed in Table 1.

ensemble model	<u>advantages</u>	<u>disadvantages</u>
1	broadly applicable to different electrode arrays; provides an overall picture of response fields, the general features of which are present in the predictions of models with far-greater complexity; computationally efficient, allowing for simulation of many conditions in a short period.	does not predict potentially-important details of response fields, primarily because (a) the model does not account for the complex voltage profiles likely to be imposed along dendrites and axons for spatially-selective electrode arrays; (b) the neural model assumes that the amplitude of the electric field at a single point is representative of the excitatory aspect of stimulation; also, the model can only account for "first-pop" responses to transient stimuli.
2	provides an approximation of voltage profiles imposed along peripheral dendrites and central axons with the UCSF electrode array; allows for the identification of nodes likely to first enter regenerative states with different waveforms and levels of excitation; allows for the computation of steady-state frequency responses and time constants of the excited nodes; allows for the simulation of effects produced by different patterns of neuron survival (e.g., for the loss of peripheral dendrites)	cannot be applied to other electrode arrays in which the heterogeneity and specific configuration of tissue impedances are likely to be important (e.g., for monopolar electrode arrays); the neural model is still crude in that it can account only for "first-pop" responses and cannot accurately predict thresholds for mammalian nodes whose characteristics are at least somewhat different from the Frankenhauser-Huxley fibers used in the McNeal model; finally, the computational efficiency of ensemble model 2 has a computational efficiency that is several orders of magnitude less than the efficiency of ensemble model 1.
3	broadly applicable to different electrode arrays and different patterns of neuron survival; multiple discharges from single neurons can be predicted for complex stimulus waveforms; complex neural phenomena such as "anodal block," "anodal break" and "AP collision" can be predicted, as can changes in sites of excitation with different stimulus waveforms and different configurations of electrodes.	computational efficiency is much lower than the efficiencies of the simpler models above; parameters of the complex models can only be roughly approximated, e.g., to (a) transform parameters for low-temperature Frankenhauser-Huxley descriptions of frog-node dynamics to parameters for mammalian myelinated fibers in the inner ear, (b) account for end conditions at the last nodes and synaptic cleft of peripheral dendrites, and (c) specify the complicated details of impedance boundaries of tissues in the ear when such boundaries and impedance values are only partly known.

STIMULUS FIELDS



NEURAL MODELS (simple strength duration)



LATENCY FIELDS (neuronal firing)

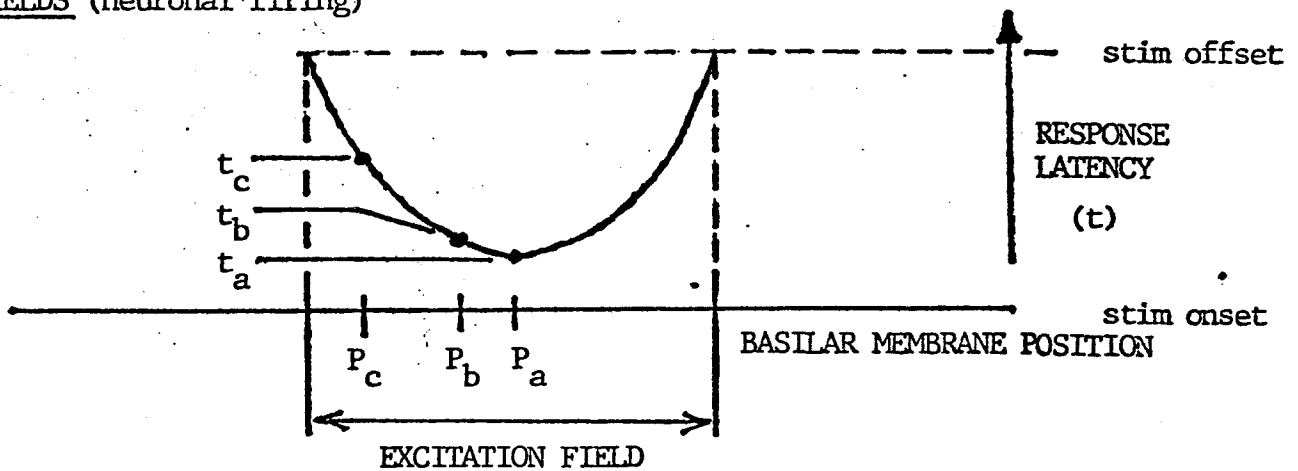


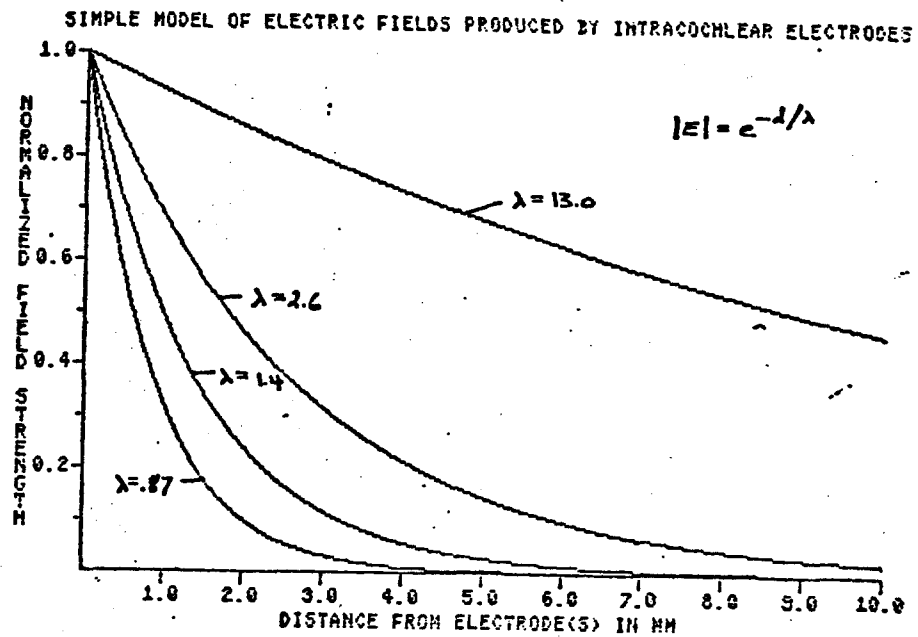
Fig. 1. Construction of a simple ensemble model of neural responses evoked by intracochlear electrical stimulation. The top panel shows an exponential falloff of electric fields for such stimulation, and the middle panel shows how strength-duration curves can be used to predict the latencies of neural responses to the imposed fields. A plot of latencies thus derived is presented in the bottom panel. This plot is the output of the ensemble model and presents, for a given set of model parameters and a given condition of stimulation, the latencies and spatial extent of evoked neural responses.

t_b , and neuron C at time t_c . These times are then used to construct the representation of "latency fields" in the bottom panel of Fig. 1. The "latency" of response is the time after pulse onset that corresponds to the instant at which the threshold of the strength-duration curve is crossed. Actual latencies would be longer than those indicated because the threshold crossing only marks the initiation of non-linear node dynamics that lead to spike discharge. However, the forms of the actual latency fields will approximate the forms of the "latency" fields shown in the bottom panel of Fig. 1.

As one might expect, a parabolic-like profile of latencies is produced by stimulation with monophasic, rectangular pulses. That is, as distance from the stimulating electrode (or electrode pair) increases, the electric field falls off and the neurons at these locations are stimulated further and further out along their strength-duration curves. Ultimately, the strength of the current field falls below threshold (for the duration of the pulse) and neurons at locations more distant than this point are not stimulated. These boundaries of the excitation field, in the two directions beyond the electrode position, are marked by vertical dashed lines in the bottom panel of Fig. 1 and by vertical dotted lines in subsequent figures.

Useful application of the simple ensemble model just described requires good estimates of (a) the space constants of electric-field falloffs for different configurations of intracochlear electrodes and (b) values of rheobase and chronaxie for auditory neurons excited by these different electrodes. Falloffs in the electric fields produced by intracochlear electrodes have been measured directly or indirectly by several investigators (e.g., Black and Clark, 1980; Merzenich and White, 1977). The results of these studies are summarized in Fig. 2, which also presents model calculations for the measured space constants. In general, monopolar stimulation produces a pervasive spread of current throughout the stimulated ear (space constant = 13 mm) and "well-positioned," radially-oriented bipolar electrodes produce a relatively-sharp falloff in the electric field (space constant = .87 mm). The range of space constants for longitudinally-oriented bipolar electrodes lies between these two extremes (typical space constant = 2.6 mm).

Although various (and sometimes quite different) techniques were used to infer the space constants for the different electrodes listed in the



lambda	remark
1.4	6 dB/mm dropoff, as found by v. Bekesy
2.0 - 4.0	4.3 - 2.2 dB/mm, as found for pseudo-bipolar stimulation by Black and Clark
0.87 - 2.8	10 - 3.3 dB/mm for stimulation of well-placed bipolar electrodes in the scala tympani, White and Merzenich, 1977
13.0	0.67 dB/mm, as found by Black and Clark for monopolar stimulation

Fig. 2. Simple model of electric fields produced by intracochlear electrodes. Space constants for exponential falloff in the modeled fields range from .87 mm to 13.0 mm. As indicated at the bottom of the figure, these values correspond to those measured for various arrangements and types of electrodes in the scala tympani.

bottom panel of Fig. 2, results of a recent study conducted by van den Honert and Stypulkowski (1985) have largely confirmed the findings of all these older studies. That is, in plots of single-unit thresholds versus characteristic frequency (which corresponds to the position of the unit's termination along the cochlear partition) for auditory nerve fibers, van den Honert and Stypulkowski find (a) a sharp drop in the thresholds of units in a highly-restricted region (approximately 1 mm) along the cochlear partition for radial bipolar stimulation, (b) a broad, sometimes multimodal, drop in thresholds with respect to cochlear position for longitudinal bipolar stimulation, and (c) essentially no spatial selectivity for monopolar stimulation. The space constants and falloff patterns presented in Fig. 2 are consistent with these findings, except that the excitatory aspect of the fields produced by longitudinal bipolar stimulation is not well-described by a simple exponential-falloff model.

While the specification of space constants for monopolar and radial bipolar stimulation is relatively straightforward, specification of rheobase and chronaxie can be complicated. Strength-duration curves for neurons stimulated by constant-current pulses delivered to intracochlear electrodes have been measured by Loeb *et al.* (1983) and by van den Honert and Stypulkowski (1984). Because measures of chronaxie and rheobase depend complexly on the voltage profiles imposed along the neuron by different types and orientations of electrodes (McNeal and Teicher, 1977; Ranck, 1975), these measurements are subject to a spatial sampling error for selective electrode arrays. To illustrate, Fig. 3 shows the chronaxies and rheobases found for 18 units responding to intracochlear stimulation in the study of van den Honert and Stypulkowski (1984, data from their Table 1, cat 179). The electrode used was an offset bipolar pair in the general configuration of such pairs in the Vienna electrode array (Hochmair-Desoyer and Hochmair, 1980). Excitation of bipolar electrodes in this configuration would be expected to produce a complex field pattern in the ear, with regions of relatively-sharp voltage gradients along peripheral dendrites (see our QPR 2, Fig. 4c). Inasmuch as sharp gradients along the dendrites are likely to lead to excitation at dendritic sites, and inasmuch as the chronaxies of dendritic stimulation are likely to be longer (maybe much longer) than the chronaxies of axonal stimulation, the rheobases and chronaxies measured with the Hochmair-type electrode are likely to reflect the heterogeneity of the electric field patterns. Specifically, one might

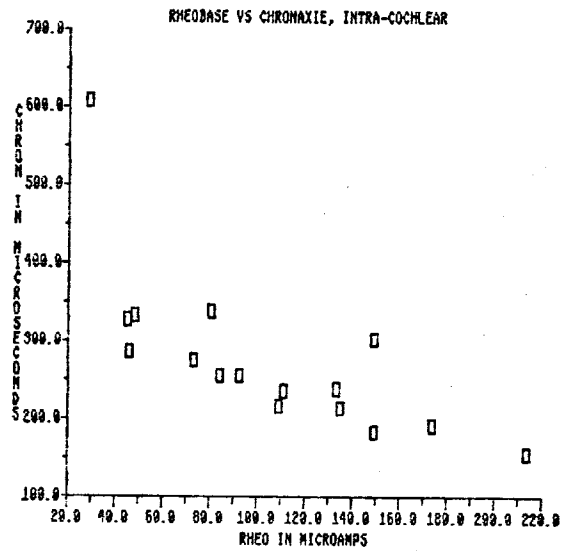


Fig. 3. Chronaxie and rheobase data reported by van den Honert and Stypulkowski (1984) for intracochlear electrical stimulation of auditory nerve fibers. The bipolar pairs of electrodes used for stimulation were similar to those described by Hochmair-Desoyer and Hochmair (1980). The least-squares regression line relating rheobase to chronaxie has a slope of -1.44 and an intercept of 426.3. The correlation is significant at the .002 level ($t = -3.86$; $df = 14$).

expect low values of rheobase and high values of chronaxie for neurons whose peripheral dendrites lie along sharp radial gradients in the electric field, and expect the opposite for neurons whose peripheral dendrites lie along gradual radial gradients in the electric field. The gradual radial gradients would induce currents through both axonal and dendritic nodes, producing an intermediate value of chronaxie, while sharp gradients would increase current flow through dendritic nodes, producing a long chronaxie.

To return now to the data of van den Honert and Stypulkowski, we see the expected relationship between rheobase and chronaxie in Fig. 3. Units with high values of rheobase have low values of chronaxie, and units with low values of rheobase have high values of chronaxie. The correlation of rheobase and chronaxie is significant at the .002 level ($t = -3.86$; $df = 14$; slope and intercept of the regression line = -1.44 and 426.3 , respectively). If the dendrite of the unit with a rheobase of about 20 lies close to the sharpest gradient in the electric field, then a chronaxie of 600 usec might be a good estimate of chronaxies of all units in this "sharp field" region. This chronaxie is much higher than the average of chronaxies presented in Fig. 3 (276 ± 104 usec). Obviously, a peaked profile of chronaxies might exist over each electrode or electrode pair of a spatially-selective electrode array, and the peak in the profile could easily be missed in the limited samples reported in the available single-unit studies. Therefore, chronaxies of neurons lying "in the middle" of spatially-selective excitation fields may be greater than the longest chronaxie reported by van den Honert and Stypulkowski, and are almost certainly much greater than the average chronaxie values reported.

The spatial sampling problem just described also complicates the interpretation of results published by Loeb et al. (1983). They monitored neural responses from large spherical cells in the low-frequency portion of the anteroventral cochlear nucleus (AVCN). The stimuli were delivered by spatially-selective bipolar pairs of electrodes positioned about halfway around the basal turn in the scala tympani. The dendrites lying in sharp-gradient regions of the fields produced by these electrodes would be those of units with high characteristic frequencies (i.e., units innervating hair cells of the basal turn have high CFs), while the units associated with the monitored AVCN cells had low characteristic frequencies. It is thus highly likely that the chronaxies reported by Loeb et al. (for 5 studied units) do not reflect the chronaxies that would be found for units whose dendrites

were in a spatially-selective region of the electric field. Indeed, one might expect "up-turn" axonal stimulation for the low-CF units studied instead of stimulation at the more-distant dendrites. In such a case, the chronaxie measured for bipolar stimulation would be consistent with excitation of axonal nodes and the chronaxie measured for monopolar stimulation (not spatially selective) would be consistent with excitation of both dendritic and axonal nodes, as outlined above. For the one unit for which a comparison between these modes of stimulation was made, the chronaxie for bipolar stimulation was 100 usec and the chronaxie for monopolar stimulation was 310 usec. The large difference in chronaxies for bipolar and monopolar stimulation emphasizes the importance of spatial aspects of the electric field on measurements of rheobase and chronaxie.

An additional complication associated with the specification of rheobase and chronaxie for model neurons is that there is strong evidence of a central shift in the sites of excited nodes with increases in stimulus intensity. That is, for all studied types of electrodes (extracochlear, monopolar; intracochlear, monopolar; intracochlear, bipolar), Stypulkowski and van den Honert (1984) find a discontinuous, downward shift in latencies of the N_1 wave in the compound action potential evoked by electrical stimulation. They attribute this shift to differences in the sites of excited nodes with different levels of stimulation. For stimuli near threshold dendritic nodes are excited, resulting in a N_1 response latency of about 0.6 msec, and for stimuli 2-to-3 times above threshold axonal nodes are excited, resulting in a N_1 response latency of about 0.3 msec. Similar shifts in latency are also found for single-unit responses to the same stimuli (van den Honert and Stypulkowski, 1984). If in fact these latency shifts reflect a central progression of excited nodes, then apparent chronaxies of excited neurons are likely to decline (perhaps precipitously) with increases in stimulus intensity.

To summarize the preceding remarks on chronaxie and rheobase, we make the following observations:

1. Reported values of rheobase and chronaxie are probably higher than actual rheobases and lower than actual chronaxies for neurons whose dendrites lie in high-radial-gradient regions of electric fields produced by spatially-selective electrodes;

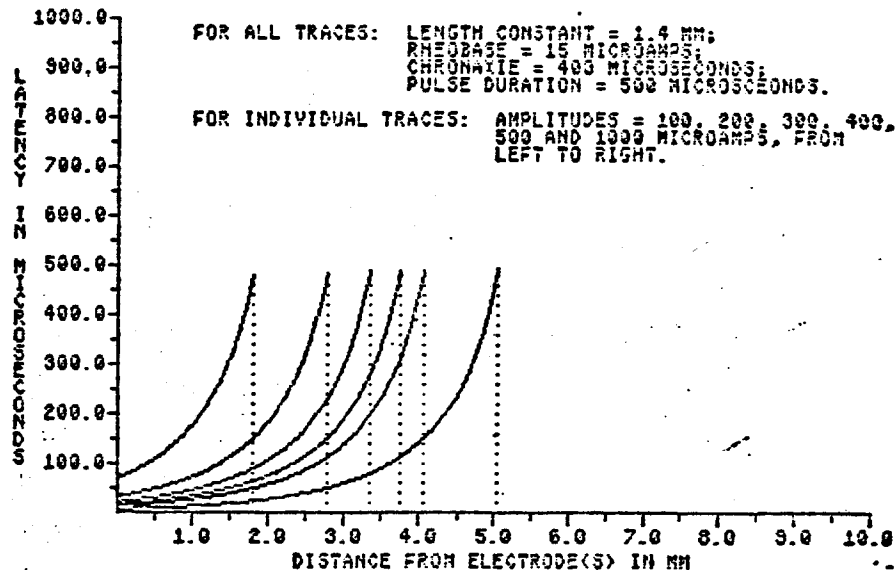
2. Reported values of rheobase and chronaxie probably approximate the actual values for electrodes that produce spatially-diffuse fields (e.g., monopolar electrodes); and
3. "Effective chronaxies" (i.e., the effective time constant of excited nodes and internodal axoplasmic resistance) are likely to undergo a large reduction when stimulus intensity is increased 2 or 3 times above the unit's threshold.

B. Effects of pulse parameters on neural response fields

To examine the general form of effects of pulse parameters on neural response fields, we have specified "typical" values for the space constant of the electric field and for the rheobase and chronaxie of model neurons. The space constant used in the simulations presented in this and the next two subsections is 1.4 mm, corresponding to moderately-well-placed electrodes with the radial orientation used in the UCSF array. The values selected for rheobase and chronaxie are 15 uA and 400 usec, respectively. These values are typical of those reported by Loeb et al. for the conditions of bipolar stimulation described in the preceding subsection. Effects of manipulating the space constant, rheobase and chronaxie will be presented in later subsections of this report. Finally, in subsections II.F and G, we will describe effects of a heterogeneous neural population on response fields elicited by bipolar and monopolar stimulation. The last subsection is one of concluding remarks, in which we will summarize observations from the preceding subsections and outline our present plan for further development and application of ensemble models.

The main effects of manipulations in pulse amplitude and duration on neural response fields are illustrated in Fig. 4. In the top panel the amplitudes of 500 usec pulses delivered to intracochlear electrodes are manipulated and in the bottom panel the durations of 200 uA pulses are manipulated. The neural response fields produced by these stimuli are indicated by the curves in each panel. Note that only one-half of the response fields is shown; for this model a symmetrical pattern of responses is present "to the left" of the electrode or electrode pair at location zero.

RESPONSE FIELDS OF NEURONS EXCITED BY INTRACOCHLEAR ELECTRODES



RESPONSE FIELDS OF NEURONS EXCITED BY INTRACOCHLEAR ELECTRODES

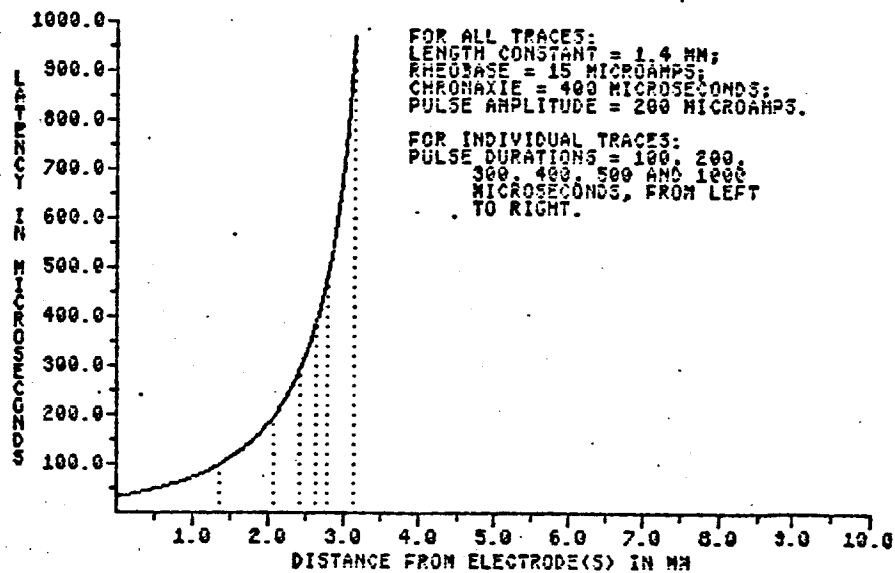


Fig. 4. Response fields of neurons excited by intracochlear electrodes, as predicted from simple models of the falloffs in electric fields produced by intracochlear electrodes and the strength-duration curves of stimulated neurons. See text for details.

Manipulations in pulse amplitude produce effects like those shown in the top panel of Fig. 4. For low-amplitude pulses a relatively-small patch of neurons is excited and for high-amplitude pulses a broader patch of neurons is excited. However, the increase in the extent of the excitation field is not a linear function of pulse amplitude; indeed, one can see a clear "compression" of growth in the excitation field with increases in stimulus intensity.

An additional effect of increases in stimulus intensity is that the shape of the latency profile is different for low-intensity and high-intensity pulses. Specifically, high-intensity pulses produce a relatively-large field of nearly-synchronous responses while low-intensity pulses do not. In the example shown in the top panel of Fig. 4, 1000 uA pulses produce a highly-synchronous response field for neurons within a distance of 2.5 mm from the electrode(s). As we will describe in subsequent subsections, such differences in latency profiles could have important perceptual correlates.

Stimulation with pulses of constant amplitude but of various durations also produces changes in the width of the excitation field, as shown in the bottom panel of Fig. 4. Again, the increase in the width of the excitation field is a nonlinear function of charge (in this case, of pulse duration and in the case of the top panel, of pulse amplitude), and the synchronicity of evoked neural activity changes as pulse duration changes. For short-duration pulses a relatively synchronous field is produced and for long-duration pulses a long "tail" of asynchronous activity is "attached" to the region of synchronous discharges in the immediate vicinity of the electrode(s).

Because all these stimuli produce relatively-synchronous excitation fields in the immediate vicinity of the electrode(s), and because only a small field of excitation is likely to be required to elicit a threshold response for an implant patient, one might expect psychophysical thresholds to lie along lines of constant charge for intracochlear stimulation. This expectation is, in fact, largely borne out by the results of many studies (see, e.g., Muller, 1983; Shannon, 1983). However, for various suprathreshold stimuli of constant charge the latency profiles and the extents of excitation can be quite different. In the next two subsections we will present some possible consequences of these differences.

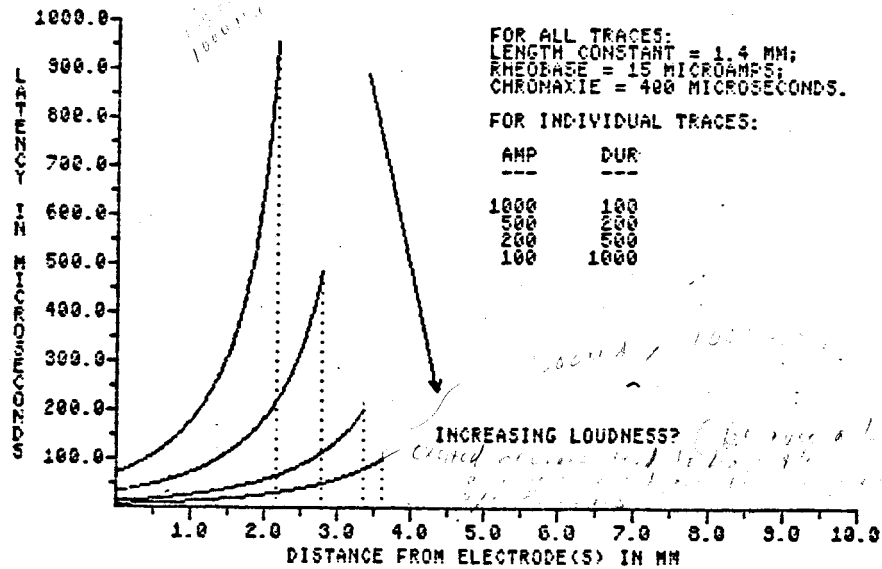
C. Manipulation of latency profiles to code stimulus intensity

The top panel of Fig. 5 shows the excitation fields predicted for constant-charge pulses of various amplitudes and durations. Decreases in duration (and increases in amplitude) produce broader, more-synchronous response fields. One might therefore expect that, for suprathreshold stimuli, short-duration pulses would be louder than long-duration pulses of the same charge. In fact, this expectation is confirmed in tests with implant patients in that perceived loudness falls off rapidly as constant-charge pulses are increased in duration from 0.1 to 1.0 msec (Shannon, 1983). In addition, these manipulations produce distinct changes in the quality of the perceived "sound" that are not the same as changes associated with simple decreases in the amplitudes of constant-duration pulses.

These model predictions and psychophysical findings suggest that either the extent of the excitation field (or total number of neurons stimulated) or the synchronicity of input or both contribute to the percept of loudness. If synchronicity of input contributes to loudness, then manipulations of the type illustrated in the bottom panel of Fig. 5 would be useful for coding the intensities of sounds for auditory prostheses. That is, intensities could be coded, at least in part, by changing the synchronicity of discharge activity over a constant-width segment of the basilar partition. By keeping the "edges" of the excitation field at constant and "constrained" positions, the spatial resolution (and interactions between adjacent channels) of stimulation could be improved. Also, if both the extent of excitation and the synchronicity of input have effects on loudness, then both can be used to increase the number of discriminable steps of loudness perception. Specifically, if "substeps" of loudness can be coded with manipulations in synchronicity for every useful step of loudness coded by extent of excitation, then the total number of steps could be increased beyond the number possible for stimulus schemes that do not exert independent control over synchronicity and extent of excitation.

The idea of coding loudness by manipulation of latency fields is further illustrated in Fig. 6. Here, the waveforms of the stimuli delivered to intracochlear electrodes are shaped to produce "flat" latency profiles across the excited patch of neurons. If both the extent of the excitation field and the synchronicity of input contribute to the percept of loudness, then percepts produced by such flat latency fields will be louder than the

RESPONSE FIELDS OF NEURONS EXCITED BY INTRACOCHELEAR ELECTRODES



RESPONSE FIELDS OF NEURONS EXCITED BY INTRACOCHELEAR ELECTRODES

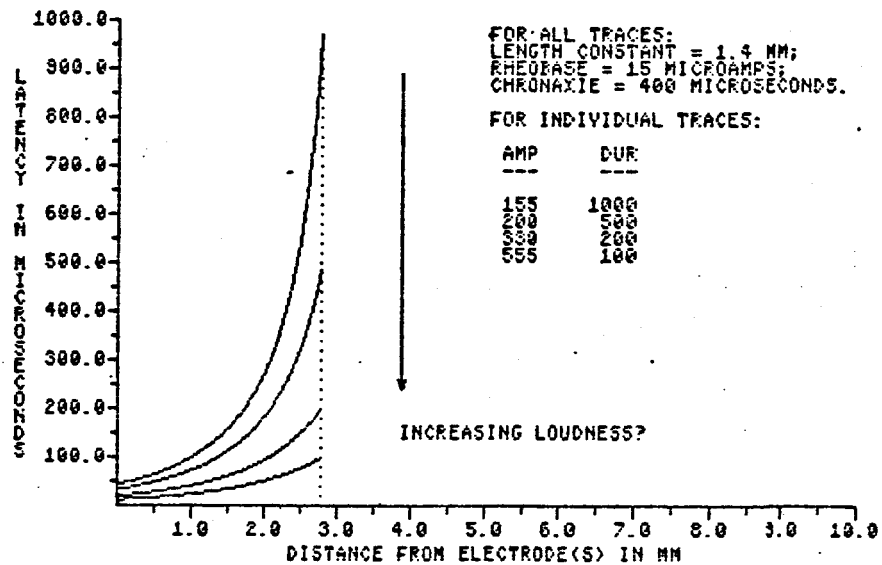


Fig. 5. Top panel: Illustration of response fields produced by constant-charge pulses. Bottom panel: Illustration of response fields produced by stimuli that maintain a constant extent of the excitation field. Note the distinct changes in the synchronicity of modeled discharge for the response fields in the bottom panel.

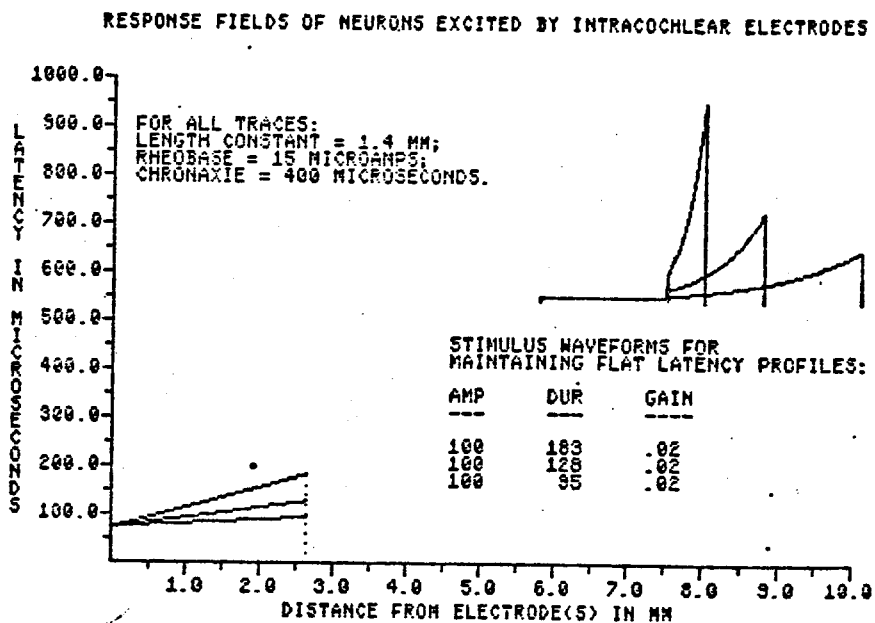
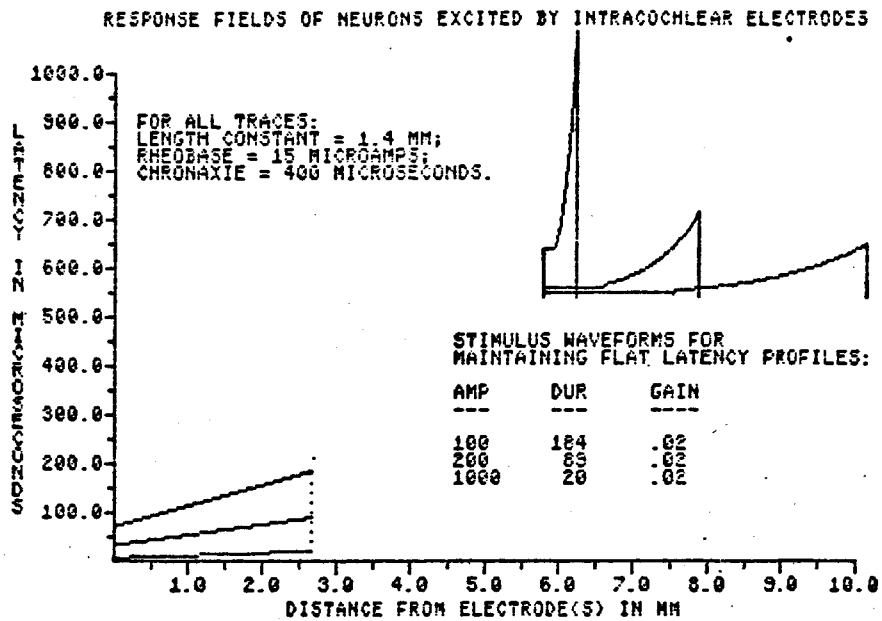


Fig. 6. Illustration of stimulus waveforms required to produce flat latency fields within a restricted region of excitation. Top panel: Waveforms with various initial amplitudes (upper right; see table for waveform parameters) required to produce flat latency profiles with various absolute latencies at the position directly over the electrode(s). Bottom panel: Waveforms with the same initial amplitude required to produce flat latency profiles with the same absolute latency at the position directly over the electrode(s).

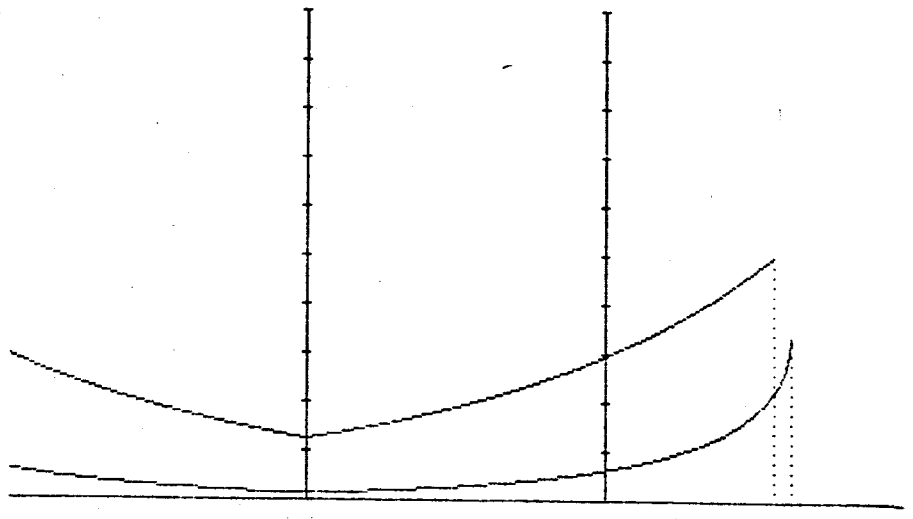
percepts produced by the curvilinear latency fields of Fig. 5.

Synchronicity and extent of excitation can also be controlled with relatively-simple stimulus waveforms. Obviously, one would not want to have to generate waveforms as complex as those shown in Fig. 6 for the outputs of speech processors for auditory prostheses. An alternative waveform that produces relatively-flat latency profiles is a rising ramp. Falling-ramp stimuli can also be used to produce a different latency profile with essentially the same extent of excitation. The predicted neural response fields for these stimuli are shown in Fig. 7. As long as the limits for safe levels of maximum current are not exceeded, such stimuli might have useful applications in auditory prostheses. Also, these stimuli can be used in psychophysical tests to evaluate the hypothesis that synchronicity of discharge across a given field of excitation contributes to the auditory percept of loudness. That is, if the loudness of suprathreshold rising ramps is the same as the loudness of falling ramps of the same charge, then the hypothesis of synchronicity of input, as just stated, will not be supported.

D. Manipulation of latency profiles to code stimulus frequency

Much recent evidence suggests the possibilities that the frequencies of sounds may be encoded at the normal auditory periphery by (1) large increases in the relative latencies of neurons whose characteristic frequencies correspond to the frequencies of components in the stimulating sound, produced by the rapid accumulation of phase lags ("phase shear") in the terminal regions of basilar-membrane displacements (see Allen, 1983; Loeb et al., 1983; Shamma, 1985a and 1985b) and (2) coincidence of temporal inputs from widely-separated segments of the cochlear partition, that could code frequency by the distance along the basilar membrane between the coincident inputs (Loeb et al., 1983). Both of these mechanisms of pitch perception have been proposed to address the problem of how a constant percept of pitch can be maintained over the very wide dynamic range of intensities for normal hearing when even moderately-intense sounds excite a broad extent of neurons along the cochlear partition. Synchronicity of "phase-locked" inputs (Sachs, 1984), phase shear and cross-correlation of widely-spaced inputs are all preserved over a much broader dynamic range

NEURAL RESPONSE (MAX LATENCY = 1000.0)
RESPONSE FIELDS TO RISING (LONGER LATENCY) AND FALLING RAMPS
(RAMP DURATION = 500 MICROSECONDS; MAXIMUM INTENSITY = 500 MICROAMPS)



Produced
Fig. 7. Neural response fields produced by rising and falling ramps. The vertical lines mark the positions of two electrode pairs in the UCSF array, which are spaced at 2 mm intervals. The graduations along the vertical lines mark 100 usec steps in "latency" after the onsets of the stimuli. The responses evoked by rising ramps have greater absolute latencies than the responses evoked by falling ramps, and the extents of the excitation fields produced by both are approximately equal.

than is the average rate profile of the responding neural population. Therefore synchronicity, phase shear and "spatial cross-correlation" are potentially robust representations of frequency that could be used by the central auditory system to infer the psychological attribute of pitch. Neural mechanisms for central "decoding" of these representations of frequency have been proposed (Loeb et al., 1983; Sachs, 1984; Shamma, 1985b). If one or more of these representations is in fact utilized by the central auditory system to infer pitch, then the deficits of pitch perception found for implant patients (see discussion below) are not at all surprising. That is, the fine temporal details of these three representations are not reproduced in the patterns of neural discharge evoked by the electrical stimuli used in present auditory prostheses. In this subsection we describe ways in which latency profiles might be manipulated to produce approximations to the representation of phase shear.

To provide a reference for subsequent discussion, an illustration of a "normal" response field evoked by a moderate-duration electrical pulse is shown in the top panel of Fig. 8. The x axis of both panels in Fig. 8 is cochlear position, as before, but includes a much larger extent of the partition than in previous figures. The eight locations along the x axis with vertical axes correspond to the positions of electrode pairs in the UCSF electrode array. The sixteen contacts of this array are indicated by electrode number in the bottom series of x-axis labels, and the positions in mm from the start of the array's spiral to the centerline of each electrode pair are indicated in the other series of x-axis labels. The spacing between the electrode pairs is approximately 2 mm. Finally, the vertical axes are all calibrated to indicate the latencies of predicted neural responses. The maximum latency for the simulation is indicated in the top label, and each y-axis graduation marks 10% of this maximum.

For the same values of space constant (1.4 mm), rheobase (15 uA) and chronaxie (400 usec) used in previous figures, we see that the response pattern shown in Fig. 8 exhibits the expected parabolic profile of latencies for pulsatile stimulation. There is a relatively synchronous region of activity immediately over the stimulated electrode(s) and long, relatively-asynchronous "tails" of activity beyond the synchronous region.

This "two-tailed" response pattern is much different from the pattern found in normal hearing. To illustrate, the bottom panel of Fig. 8 shows the pattern of normal hearing superposed on the pattern predicted for

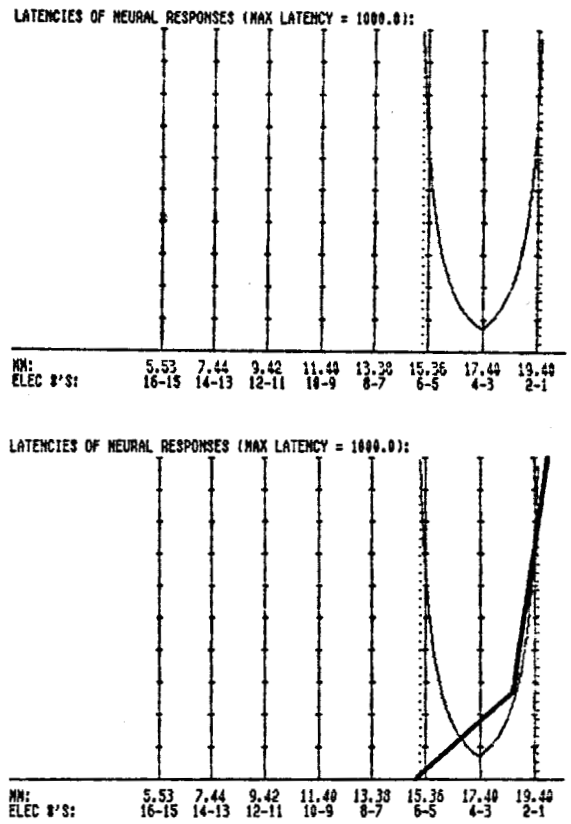


Fig. 8. Top panel: response field evoked by 100 μ A, 1000 μ sec monophasic pulse for the following model parameters: $\lambda = 1.4$ mm; rheo = 15 μ A; chron = 400 μ sec. The x axis of both panels is calibrated in units of cochlear position. The eight locations along the x axis with vertical axes correspond to the positions of electrode pairs in the UCSF electrode array. The sixteen contacts of this array are indicated by electrode number in the bottom series of x-axis labels, and the position in mm from the start of the array's spiral to the centerline of each electrode pair are indicated in the other series of x-axis labels. The vertical axes are all calibrated to indicate the latencies of predicted neural responses, with the maximum latency indicated in the top label for each panel. Bottom panel: the latency profile found in normal hearing for a 1500 Hz tone is superposed on the latency profile predicted for electrically-evoked hearing.

electrically-evoked hearing. The pattern for normal hearing is a consequence of basilar-membrane mechanics. Specifically, for a given frequency component in an acoustic stimulus, propagation of disturbances along the basilar membrane is rapid for positions basal to the place corresponding to this frequency, and propagation is progressively slowed as this place is approached and passed. The accumulation of phase lags in the "terminal region" surrounding the place of the stimulus frequency is well approximated by a straight-line segment of about 540° /octave, and the accumulation of phase lags basal to this region is well approximated by a straight-line segment of about 90° /octave (Kim et al., 1980, Figs. 3 and 6; Synder and Schreiner, 1985, p. 59). These two segments are plotted in Fig. 8 for a stimulus frequency of 1500 Hz. The place corresponding to the stimulus frequency lies near the middle of the apical, high-slope segment.

If the central auditory system attends to the latency profiles produced in normal hearing to infer pitch (see above), then the profiles produced in electrically-evoked hearing are likely to elicit some unusual pitch percepts. For example, if lateral inhibitory networks (LINs) in the central system serve to identify regions of latency "breaks" and large increases in latencies, as Shamma (1985b) has argued, then both long-latency "tails" in the response field evoked by electrical pulses would be detected as regions corresponding to frequencies of input "sound." In fact, depending on the topology and time constants of the LINs, the basal, "reverse-latency" tail could produce a larger output than the apical, "normal-latency" tail. In such an instance we would expect that (a) a complex pitch percept would be elicited, with at least two "components" corresponding to the positions of the tail regions, (b) these components would generally be inharmonically related, (c) the relation between the two (or more, see subsection II.F below) components would change with manipulations in pulse intensity and duration (see Fig. 4), producing complex changes in the pitch percept, and (d) the "overall" percept of pitch might increase with increases in stimulus intensity inasmuch as the basal tail could produce a more-salient input for the central system, as described above.

Because pitch percepts evoked by intracochlear electrical stimulation are uniformly described as much more complex than "pure-tone" percepts of normal hearing (see, e.g., Shannon, 1983), and because the pitch percepts of electrically-evoked hearing generally increase with increases in stimulus intensity (Pfingst et al., 1985; Shannon, 1983; Simmons et al., 1979), the

predictions stated above seem to be largely consistent with psychophysical findings. Therefore, a better approximation of the latency fields found in normal hearing might produce more-salient and less-complex percepts of pitch for cochlear implant patients.

One approach toward such an approximation is illustrated in Fig. 9. Here the two-segment latency fields of normal hearing are mimicked by delivering a high-intensity, short-duration pulse to one electrode (or electrode pair) and a low-intensity, long-duration pulse to the electrode (or electrode pair) immediately apical to the first electrode. Current summation between the channels produces a continuous field of excitation, with the short-duration pulse dominating the field over the basal electrode and the long-duration pulse dominating the field over the apical electrode. The result is a relatively-synchronous field at basal locations coupled with a single asynchronous tail just beyond the apical electrode. If the central auditory system "reads" latency breaks (by whatever mechanism) to infer pitch, then response fields like those shown in Fig. 9 should eliminate the complicating influence of the second (basal) latency tail found in electrically-evoked hearing for single pulses.

In addition to illustrating a basic strategy for approximating the latency fields of normal hearing, Fig. 9 shows that this strategy is robust over wide ranges of stimulus parameters and spatial selectivities of excitation. Further, within these ranges the location of the asynchronous tail can be moved in an apicalward or basalward direction with certain manipulations of stimulus parameters. Such control may provide a way in which the frequencies of input sounds can be coded along a continuous dimension of cochlear position.

E. Illustration of temporal channel interactions

In the last subsection we demonstrated a way in which interactions between channels might be exploited to code a dimension of the auditory stimulus. In this subsection we will briefly show how channel interactions can be destructive to the representation if left uncontrolled.

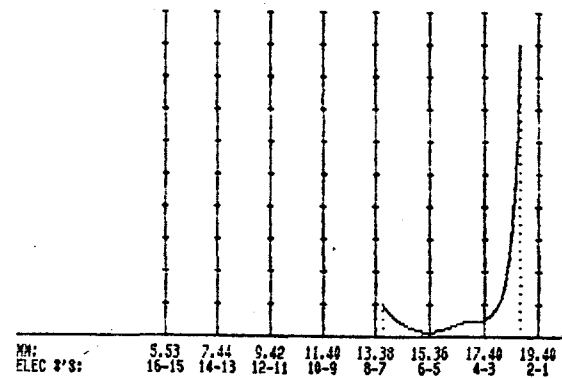
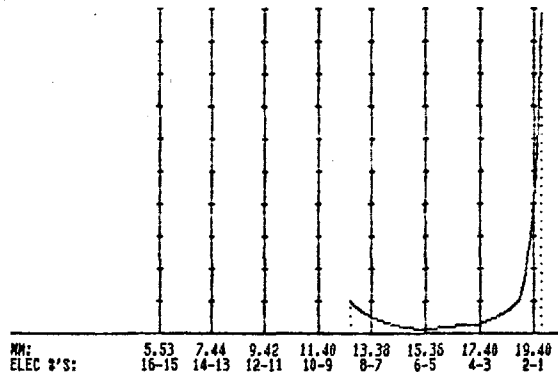
Illustrations of channel interactions produced by simultaneous stimulation of adjacent electrodes or pairs of electrodes are presented in Fig. 10. The upper, parabolic-like curves in each panel show the neural

$\lambda = 1.4 \text{ mm}$

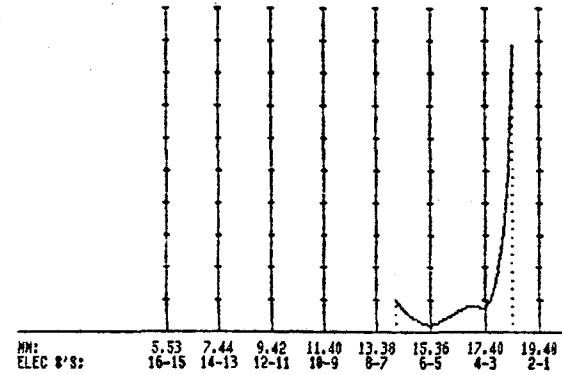
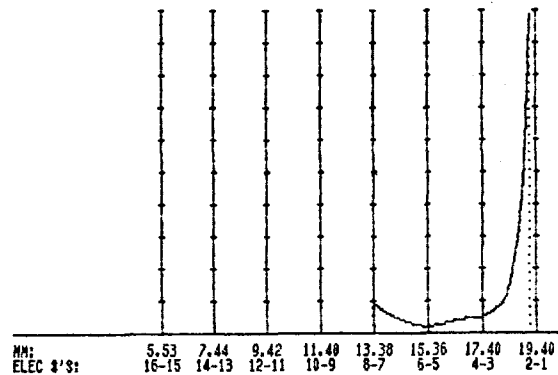
$\lambda = 0.87 \text{ mm}$

Stimuli

6-5: 500 μA ,
100 μsec
4-3: 100 μA ,
1000 μsec



6-5: 300 μA ,
100 μsec
4-3: 70 μA ,
1000 μsec



6-5: 200 μA ,
100 μsec
4-3: 60 μA ,
1000 μsec

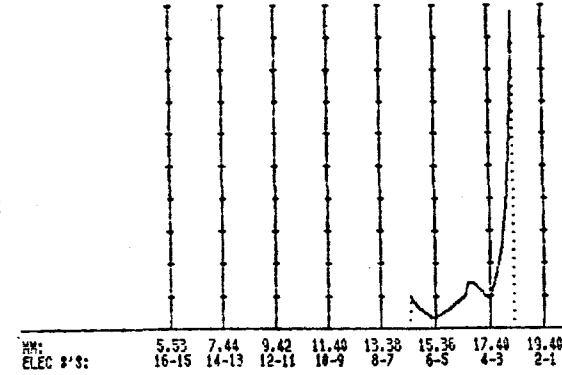
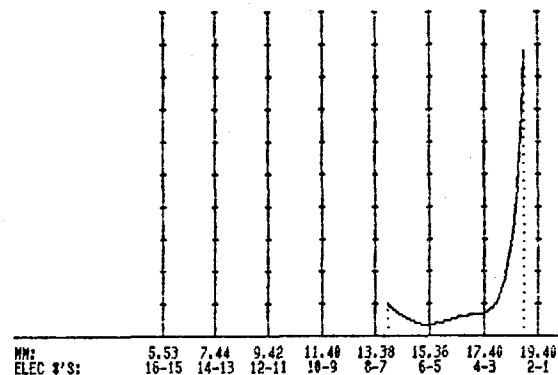


Fig. 9. Predicted latency fields for short-duration, high-intensity pulses delivered to electrode pair 6-5 in combination with long-duration, low-intensity pulses delivered to electrode pair 4-3. The space constant for the left column of panels is 1.4 mm, and the space constant for the right column of panels is 0.87 mm. Rheobase is 15 μA and chronaxie is 400 μsec for all panels. The maximum latency for all panels is 1000 μsec . The sharp discontinuities in the latency fields approximate the discontinuities found in normal hearing.

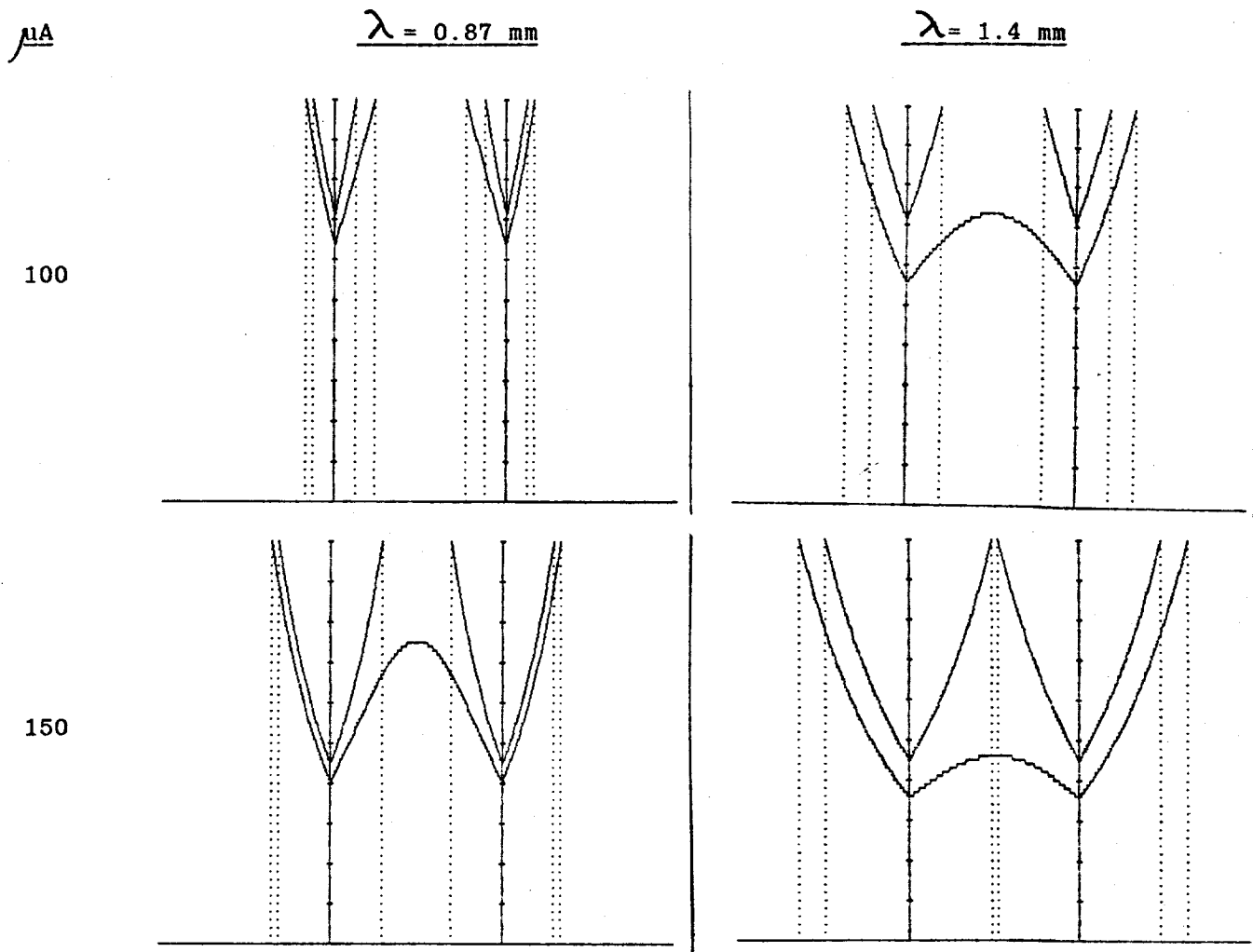


Fig. 10. Illustrations of channel interactions produced by simultaneous stimulation of adjacent electrodes or pairs of electrodes. The upper, parabolic-like curves in each panel show the neural response fields predicted for stimulation of only one electrode or electrode pair at a time. The stimuli are 100 μ sec monophasic pulses with the amplitudes indicated in the left column of numbers. As in previous figures, the neural properties are: rheobase = 15 μ A; and chronaxie = 400 μ sec. The space constants of the electric field are 0.87 mm for the left column of panels and 1.4 mm for the right column of panels. The vertical axes in each panel indicate the positions of the electrodes (which are 2 mm apart), and each calibration mark on these axes indicate 10 μ sec of latency. Finally, the lower curves in each panel show the neural response fields predicted for simultaneous stimulation of both electrodes (or electrode pairs). Note that simultaneous stimulation of adjacent channels can produce excitation fields that are much broader than the two separate fields produced by nonsimultaneous stimulation.

response fields predicted for stimulation of only one electrode (or electrode pair) at a time. These fields do not overlap for the conditions shown in Fig. 10. In contrast, for three of four conditions of simultaneous stimulation, shown in the lower curves of each panel, a continuous field of excitation is produced between and beyond the two electrodes. In general, the fields produced by simultaneous stimulation are much broader than the fields produced by nonsimultaneous stimulation. The extent of interaction depends complexly on the parameters of the stimuli and on the spatial selectivity of the electric field. In all cases, however, temporal summation of the electric field between and beyond the electrodes substantially increases the width and alters the latency pattern of the neural excitation field.

In terms of the design of speech processors for auditory prostheses, the growth of the excitation field between electrodes is obviously destructive to a representation of discrete stimulation of neural populations over each electrode in a multichannel array. One strategy to avoid this destructive effect was presented in our last quarterly report, and consisted of a simple interlacing of pulses delivered to separate bipolar pairs of electrodes in the UCSF array. Psychophysical measurements of the time constants of temporal summation within and between channels for the patient described in this last QPR indicated that little summation occurred for pulses separated by 1 msec or more. Therefore, pulses were delivered to one channel (i.e., one bipolar pair of electrodes) at a time, and the minimum time between the offset of a pulse delivered to one channel and the onset of the next pulse delivered to another channel was set at 1 msec. As described in detail in QPR 7, this strategy produced immediate and compelling improvements in speech recognition over strategies that delivered simultaneous outputs to different channels. We believe that control of temporal channel interactions is one of the more-important considerations in the design of advanced speech processors for auditory prostheses.

F. Effects of a heterogeneous neural population on response fields elicited by bipolar and monopolar stimulation

Model neurons used in all previous simulations of this report have had a single value of rheobase (15 uA) and a single value of chronaxie

(400 usec). As reviewed in some detail in section II.A, however, neurons in the cochlea comprise a heterogeneous population, in which (a) the values of rheobase and chronaxie depend on the configuration and placement of the stimulating electrodes and (b) the "effective chronaxies" depend on the level of stimulus intensity above threshold. An additional factor that might be reflected in the values of rheobase and chronaxie is the location of dendrites in the complex electric fields produced by spatially-selective electrodes. Specifically, neurons whose dendrites lie along sharp radial gradients of the electric field are likely to exhibit lower rheobases and higher chronaxies than neurons whose dendrites do not lie along such gradients. Finally, values of rheobase and chronaxie could be profoundly affected by neural pathology. One would expect, for example, a reduction in chronaxies for neurons whose peripheral dendrites are absent or otherwise pathological.

In this subsection we will examine effects of introducing variability in the simulated population of model neurons. In particular, we will show that (a) the basic properties of responses described in previous subsections are also found in the responses of a heterogeneous neural population, (b) there are striking differences in the patterns of responses elicited with electric fields with the spatial selectivities of bipolar and monopolar stimulation, (c) despite these differences good localization of neural activity over the stimulating electrodes can be obtained for both bipolar and monopolar excitation, and (d) presumed excitation of axonal nodes at 2-to-3 times the threshold for dendritic nodes can affect the response fields evoked by bipolar stimulation, especially for short-duration pulses. Among these findings point c is most surprising, and we will therefore explore this effect in some detail.

As a starting point for examining effects of a heterogeneous neural population, 10 model neurons are included at each spatial step in the ensemble model, and each of these neurons is assigned a different value of rheobase. The range of rheobase values is selected to approximate the total, 4-to-1 range in thresholds found by van den Honert and Stypulkowski (1984) for monopolar stimulation of the cat ear. Specifically, a 2-to-1 range in rheobase values approximates a 4-to-1 range in thresholds across unit characteristic frequency (i.e., across the extent of the cochlea) for the gentle falloffs in the electric field produced by monopolar stimulation. The rheobase values of neurons in the simulations of Figs. 11-14 are 20, 22,

24, 26, 28, 30, 32, 34, 36 and 38 uA. As before, the chronaxie for all neurons is 400 usec.

Predicted neural response fields for stimulation with 100 and 1000 usec monophasic pulses are presented in Figs. 11 and 12. Fig. 11 shows the expected patterns for electrodes with a high degree of spatial selectivity (space constant = 0.87 mm) and Fig. 12 shows the expected patterns for electrodes with a low degree of spatial selectivity (space constant = 13.0 mm). The levels of stimulation in the left panels of both figures are those required to elicit 150 responses from the model neurons for 100 and 1000 usec pulses, and the levels of stimulation in the right panels of both figures are those required to elicit 450 responses from the model neurons. Finally, the representation of latency and cochlear position is the same as that in Figs. 8 and 9.

Examination of Fig. 11 demonstrates that a family of neural response curves is produced for each condition of stimulation. In all cases the curves of individual neurons are tightly clustered, and each curve exhibits the parabolic-like shape of previous figures. The cochlear extent of the widest response curve for both the "150 responses" panels is 1.2 mm and the cochlear extent of this curve for the "450 responses" panels is 2.4 mm. If the total number of responding neurons is a determinant of loudness, which is likely, then neural response fields like those in the "150 responses" panels are probably correlated with suprathreshold sensations in cochlear-implant patients and response fields like those in the "450 responses" panels are probably correlated with much-louder sensations. All patterns of responses for electrodes with a space constant of 0.87 mm are confined to the immediate vicinity of the stimulating electrode(s). Also, for the conditions of stimulation presented in Fig. 11, all ten model neurons are responding over some (usually restricted) extent of the excitation field.

Comparison of Figs. 11 and 12 shows that the response fields predicted for monopolar stimulation (Fig. 12) are quite different from the response fields predicted for bipolar stimulation (Fig. 11). In particular, the response fields for monopolar stimulation are much broader in spatial extent. Also, as might be expected from the broader response fields, the "density" of neural responses (i.e., the total number of responding neurons at each spatial position) is in general much lower than in the bipolar cases. The greatest density for the conditions of Fig. 12 is 4 responding neurons immediately over the electrode (for the "450 responses" panels) and

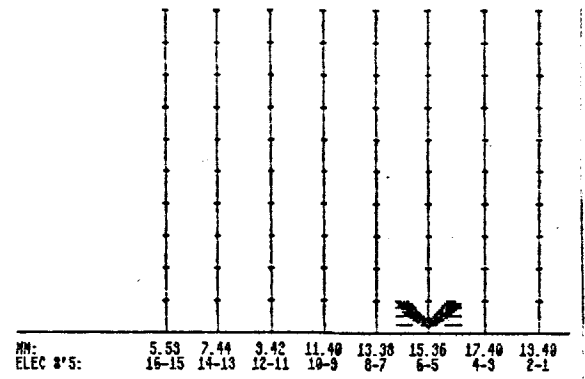
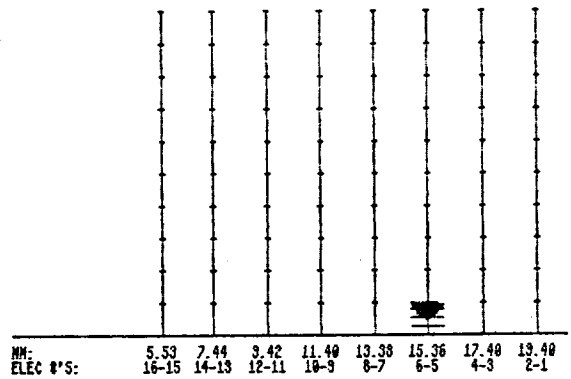
$$\lambda = 0.87 \text{ mm}$$

duration

150 responses

450 responses

100 μ sec



1000 μ sec

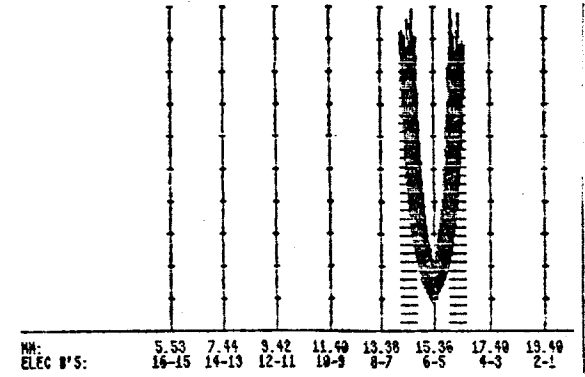
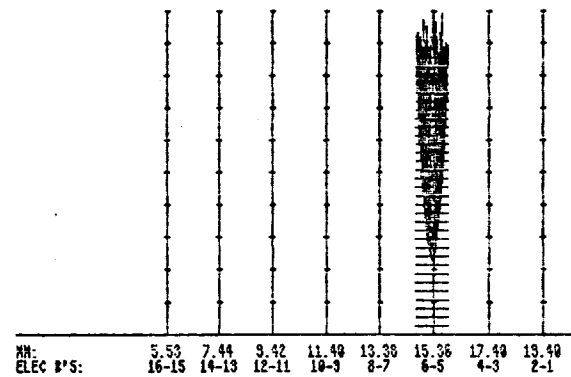


Fig. 11. Predicted neural response fields for stimulation with 100 and 1000 μ sec monophasic pulses. The space constant of the electric field is 0.87 mm and approximates that of well-positioned bipolar electrodes of the UCSF electrode array. To simulate the known variability of parameters describing auditory neurons, ten neurons are modeled at each spatial position with rheobase values of 20, 22, 24, 26, 28, 30, 32, 34, 36 and 38 μ A. The chronaxie for all neurons is 400 μ sec, and the maximum latency for all panels is 1000 μ sec. The stimulus levels required to elicit responses from 150 model neurons are 200 μ A for 100 μ sec pulses and 56 μ A for 1000 μ sec pulses; these levels for 450 responses are 400 μ A for 100 μ sec pulses and 112 μ A for 1000 μ sec pulses. Note that the variability of neural properties produces a family of neural response curves, each of which has the parabolic-like shape of curves presented in previous figures.

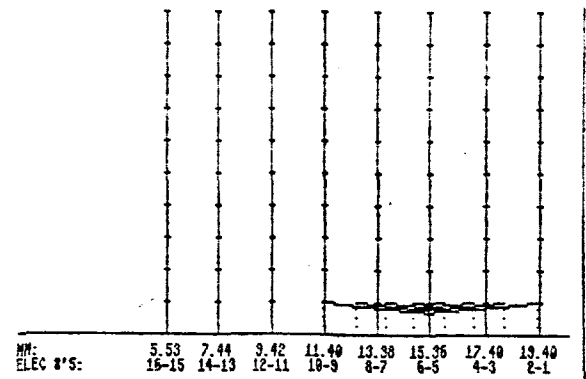
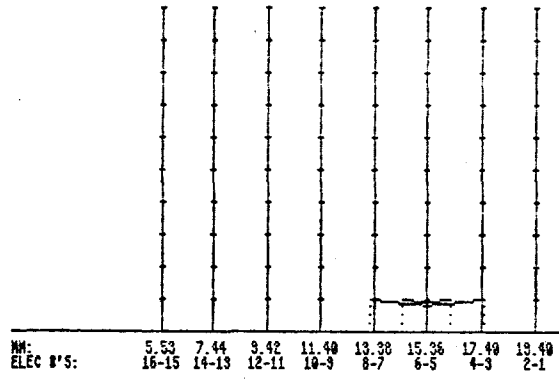
$$\lambda = 13.0 \text{ mm}$$

duration

150 responses

450 responses

100 μsec



1000 μsec

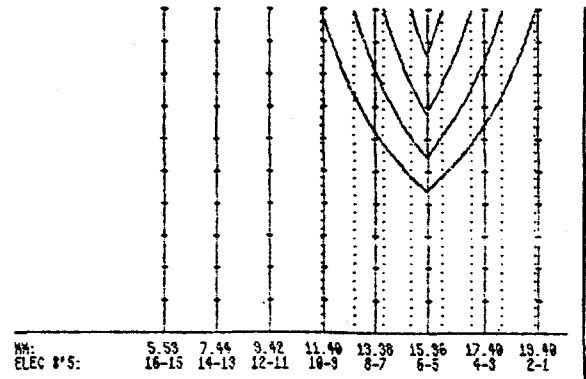
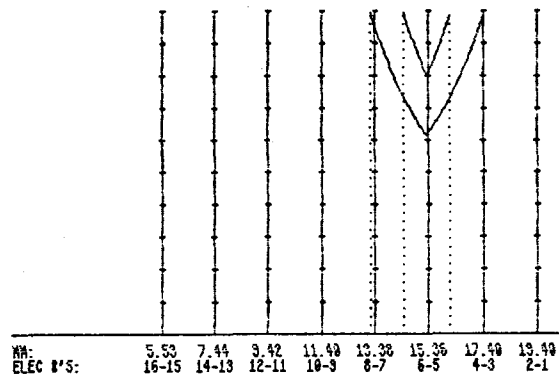


Fig. 12. Predicted neural response fields for stimulation with 100 and 1000 μsec monophasic pulses. The space constant of the electric field is 13.0 mm and approximates that of monopolar electrodes. The properties of model neurons and the format of information in this figure are specified in the caption of Fig. 11. The stimulus levels required to elicit responses from 150 model neurons are 117 μA for 100 μsec pulses and 32.9 μA for 1000 μsec pulses; these levels for 450 responses are 135 μA for 100 μsec pulses and 38.0 μA for 1000 μsec pulses. Note the greater spreads in the latencies and widths of the excitation fields for monopolar stimulation (this figure) compared with the spreads for bipolar stimulation (Fig. 11).

the greatest density in all panels of Fig. 11 is 10 responding neurons over the electrodes. Therefore, to reach criterion levels of total response, monopolar stimulation selectively excites low-threshold neurons while bipolar stimulation does not.

A consequence of such selective excitation (according to unit threshold), and of the greater dispersion of individual response curves produced by monopolar stimulation, is illustrated in Fig. 13. Here, the patterns of responses predicted for four intensities of 100 usec pulses are presented in the left column of panels. The response fields produced by the most-intense stimulus (200 uA, bottom left panel) would be expected to elicit an extremely-loud auditory percept.

The densities of neural responses, along with the profile of the electric field, are presented in the right column of panels in Fig. 13. The surprising aspect of the density profiles is that they are much sharper than the profile of the electric field, over a broad range of stimulus intensities. This sharpening of the neural density profile may explain how patients implanted with monopolar arrays can rank their electrodes (see, e.g., Eddington et al., 1978). It may also explain how both humans and monkeys (Pfungst et al., 1985) can rank monopolar electrodes over a broad dynamic range of stimulation (and not just at threshold). In Fig. 13, for example, the neural density profile remains sharp up to 150 uA of stimulation, which would probably correspond to a loud percept for both species.

To provide a comparison of neural density profiles produced by monopolar electrodes and spatially-selective electrodes, Fig. 14 shows the profiles predicted for electrodes with a space constant of 0.87 mm. The profile is sharper than the electric field at low stimulus intensities and is about as sharp as the electric field at moderate stimulus intensities. The "crossover point," at which the sharpness of the neural density profile approximates the sharpness of the electric field, is lower with bipolar stimulation than with monopolar stimulation because monopolar stimulation selectively excites low-threshold neurons.

Equivalent space constants of the neural density profiles shown in Figs. 13 and 14 are presented in Table 3. As would be expected from the previous remarks, the equivalent space constants of the neural density profile are substantially less than the space constant of the electric field for monopolar stimulation. At moderate intensity levels, for example, the

$$\lambda = 13 \text{ mm}$$

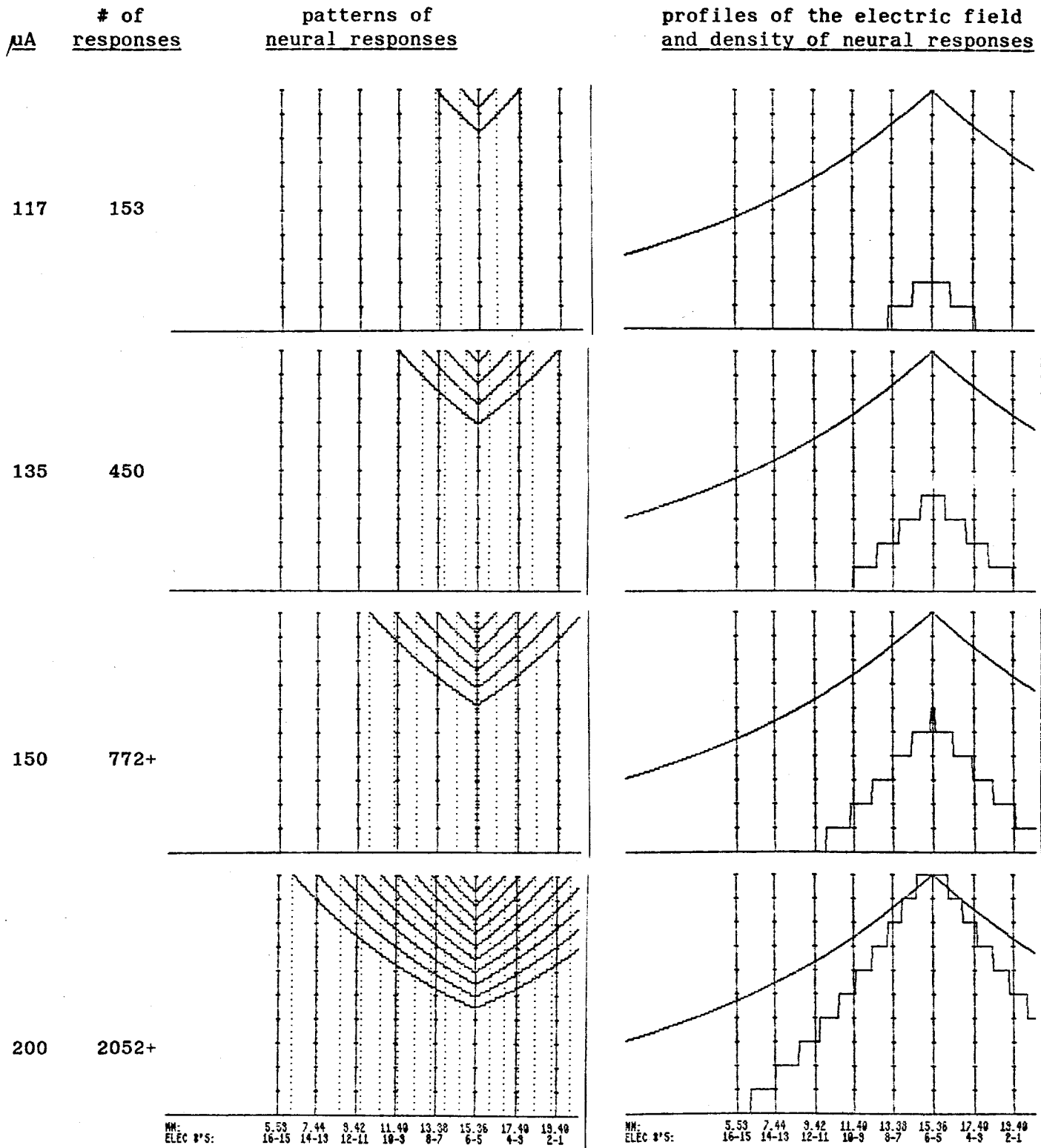


Fig. 13. (caption on next page)

Fig. 13. Growth of neural excitation fields with increases in the intensities of 100 μ sec monophasic pulses. The space constant of the electric field is 13 mm and approximates that of monopolar electrodes. Ten neurons are modeled at each spatial position with rheobase values of 20, 22, 24, 26, 28, 30, 32, 34, 36 and 38 μ A. The chronaxie for all neurons is 400 μ sec. Stimulus intensities are indicated in the leftmost column of numbers, and the total numbers of neural responses found for each stimulus condition are indicated in the next column of numbers. Entries with a "+" symbol indicate the total number of responses along the extent of the cochlear partition shown; additional responses not shown are elicited in the apical direction for these conditions of stimulation. Note that the sharpness of the excitation, as measured by the density of neural responses with respect to position (rightmost column of panels), is (1) relatively constant over a broad dynamic range of stimulation and (2) substantially sharper than the falloff in the electric field profile.

$$\lambda = 0.87 \text{ mm}$$

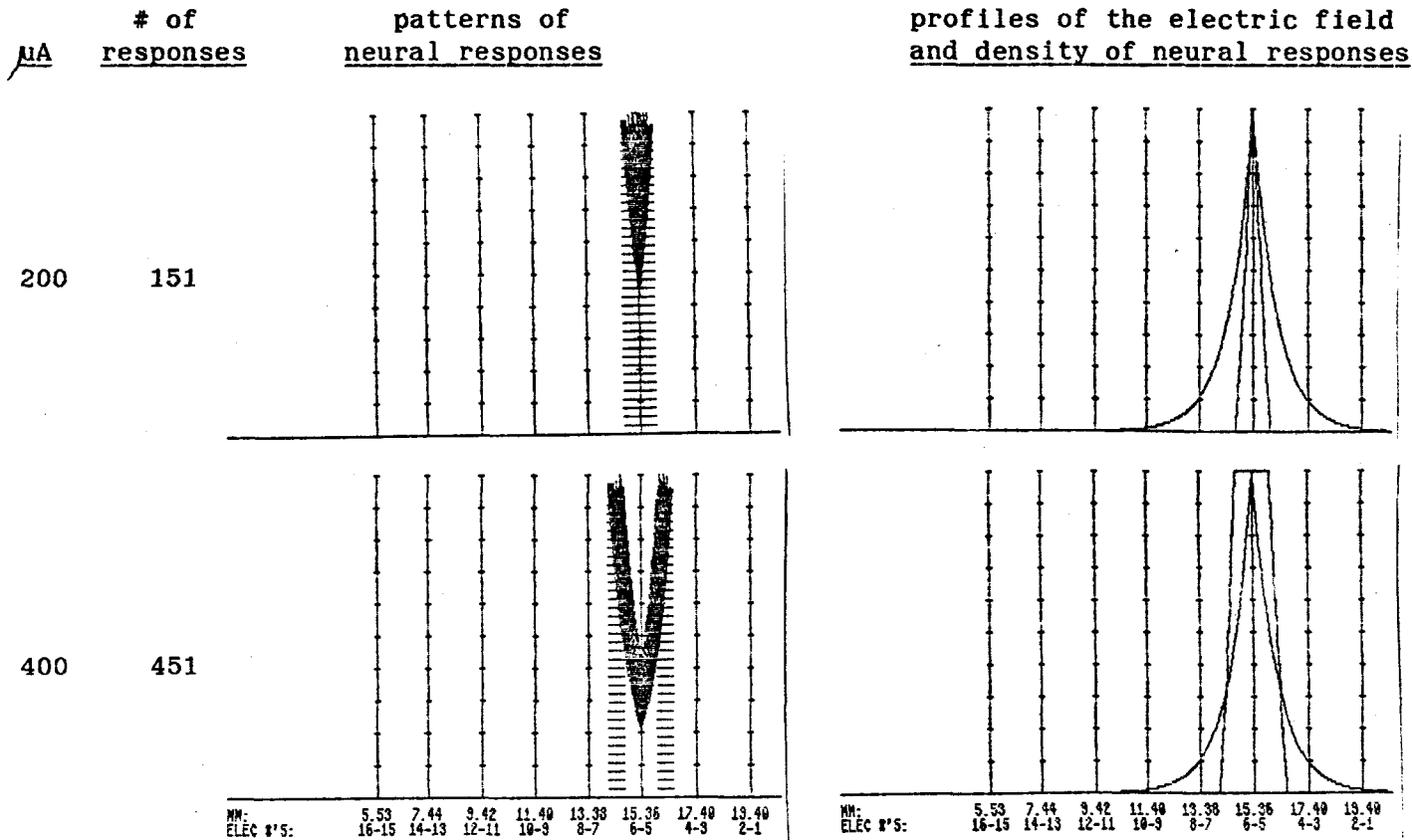


Fig. 14. Growth of neural excitation fields with increases in the intensities of 100 μsec monophasic pulses. The space constant of the electric field is 0.87 mm and approximates that of well-positioned bipolar electrodes of the UCSF electrode array. The properties of model neurons and the format of information in this figure are specified in the caption of Fig. 13. Note that the sharpness of the excitation for $\lambda = 0.87$ mm is not constant over the dynamic range of stimulus intensities presented in this figure. The excitation field is very sharp for low stimulus intensities and somewhat less sharp than the electric-field profile at high stimulus intensities.

Table 3. Comparison of space constants for the electric field and the density profile of evoked neural responses.

λ of the electric field (mm)	stimulus intensity (uA)	# of responses	equivalent λ^* of the excitation field (mm)
13.00	117	153	2.0
	135	450	3.6
	150	772+	3.4
	200	2052+	5.7
0.87	200	151	0.4
	400	451	0.9

*Equivalent λ is defined as one-half the width of the excitation profile at the level equal to 37% of the peak in the profile.

equivalent space constant of the neural density profile is about 3.5 mm, which is a factor of 3.7 below the space constant of the electric field (13 mm). The equivalent space constant of the neural density profile for bipolar stimulation at moderate intensity levels is about 0.9 mm, roughly the same as the space constant for the electric field (0.87 mm). Although the equivalent space constant of 0.9 mm for bipolar stimulation is much lower than the 3.5 mm for monopolar stimulation, both values indicate spatially-selective excitation of overlying populations of neurons.

An additional variation in response patterns produced by a heterogeneous neural population is illustrated in Fig. 15. The conditions of this figure are the same as those in Fig. 11, except that the model neurons in Fig. 15 are designed to simulate a reduction in "effective chronaxie" when stimulus intensities are raised 2-to-3 times above threshold. The situation modeled is that described by Stypulkowski and van den Honert (1984), of a central progression of excited nodes in electrically-evoked responses with increases in stimulus intensity (see section II.A for discussion). At low intensities the data of Stypulkowski and van den Honert indicate that dendritic nodes are excited and at high intensities axonal nodes are also excited. Because the axonal sites are central to the dendritic sites, the properties of axonal nodes are reflected in responses evoked by stimuli 2-to-3 times above the threshold of dendritic activation.

To simulate possible effects of axonal-node activation, two sets of rheobase and chronaxie values are assigned to the 10 model neurons at each spatial step in the ensemble model. The values for dendritic activation are the same as those used in previous figures of this subsection (Figs. 11-14). The "effective" values for axonal activation are: chronaxies of 118 usec for all neurons, and a range of rheobases from 68 to 77 uA, in steps of 1 uA, for each neuron. These values simulate (a) the average chronaxie of axonal stimulation found by van den Honert and Stypulkowski (1984) for laminectomy preparations, (b) the lower degree of variability found by these investigators in responses resulting from axonal stimulation, and (c) the suprathreshold levels required for such stimulation. Finally, the absolute latencies of responses evoked by axonal activation are about 200 usec less than the latencies of responses evoked by dendritic activation; this aspect of the response fields is also incorporated into the "multinodal" model of Fig. 15.

$\lambda = 0.87$ mm; two sites of excitation

duration

Previous levels for
150 responses

Previous levels for
450 responses

100 μ sec

PATTERN OF RESPONDING NODES (TOP = MED; MID = MID; BOT = LAT):

PATTERN OF RESPONDING NODES (TOP = MED; MID = MID; BOT = LAT):

LATENCIES OF NEURAL RESPONSES (MAX LATENCY = 1200.0):

LATENCIES OF NEURAL RESPONSES (MAX LATENCY = 1200.0):

MM:	5.53	7.44	9.42	11.40	13.38	15.36	17.40	19.40
ELEC #'S:	16-15	14-13	12-11	10-9	8-7	6-5	4-3	2-1

MM:	5.53	7.44	9.42	11.40	13.38	15.36	17.40	19.40
ELEC #'S:	16-15	14-13	12-11	10-9	8-7	6-5	4-3	2-1

PATTERN OF RESPONDING NODES (TOP = MED; MID = MID; BOT = LAT):

PATTERN OF RESPONDING NODES (TOP = MED; MID = MID; BOT = LAT):

LATENCIES OF NEURAL RESPONSES (MAX LATENCY = 1200.0):

LATENCIES OF NEURAL RESPONSES (MAX LATENCY = 1200.0):

MM:	5.53	7.44	9.42	11.40	13.38	15.36	17.40	19.40
ELEC #'S:	16-15	14-13	12-11	10-9	8-7	6-5	4-3	2-1

MM:	5.53	7.44	9.42	11.40	13.38	15.36	17.40	19.40
ELEC #'S:	16-15	14-13	12-11	10-9	8-7	6-5	4-3	2-1

1000 μ sec

Fig. 15. (caption on next page)

Fig. 15. Predicted neural response fields for the conditions of Fig. 11, except that the model neurons in the present figure are designed to simulate a reduction in "effective chronaxie" when stimulus intensity is raised 2-to-3 times above threshold. Specifically, rheobase values for "axonal" stimulation range from 68 to 77 μ A in steps of 1 μ A, to simulate (1) the lower degree of variability for axonal stimulation and (2) the suprathreshold (over presumed excitation of dendritic nodes) levels required for such stimulation. The chronaxie for axonal stimulation is 118 μ sec. Values of rheobase and chronaxie for dendritic activation are the same as those in Fig. 11. In each panel of the present figure the site of activation is indicated in the top set of horizontal bars. The upper bars in the 100 μ sec panels and the rightmost 1000 μ sec panel show the spatial extents of axonal-node stimulation, and the lower bars in all panels show the spatial extents of dendritic activation. Note that the percentage of axonal stimulation increases with increases in pulse intensity and decreases in pulse duration. Finally, the stimulus levels used in Fig. 11, to produce 150 and 450 responses for 100 μ sec pulses, produced 163 and 463 responses in the 100 μ sec simulations of the present figure. The simulations for 1000 μ sec pulses produced the same number of responses in both figures.

The results presented in Fig. 15 show that excitation of axonal nodes can alter the response fields produced by spatially-selective electrodes. In particular, most responses evoked by short-duration pulses arise from stimulation at axonal nodes. This is an expected result inasmuch as the effective chronaxie for axonal stimulation is about four times lower than the chronaxie for dendritic stimulation. Also, high-intensity pulses can excite axonal nodes even at long pulse durations. This effect can be seen in the lower-right panel of Fig. 15, in which a small, short-latency "tip" is evident in the responses immediately around the electrode(s).

Practical consequences of axonal stimulation include (a) the introduction of latency discontinuities at the boundaries of axonal and dendritic stimulation; (b) a slight broadening of the excitation field over that of dendrite-only activation; and (c) a reduction in the variability of neural responses evoked by intracochlear electrodes. In terms of the design of speech processors for auditory prostheses, these consequences may have degrading effects. Possible effects related to point (a) above will be described in the last paragraphs of this subsection and possible effects related to point (c) above will be described in the next subsection.

The final aspect of responses from a heterogeneous population we want to consider in this subsection is how heterogeneity might alter the basic properties of responses previously described for uniform populations of neurons. First, we note that responses from heterogeneous populations consist of a family of single-neuron curves. These curves are tightly clustered for spatially-selective electrodes (Fig. 11). Therefore, the previous remarks on manipulation of latency profiles to code stimulus attributes (sections II.C and D) and on temporal channel interactions (section II.E) generally apply to responses evoked from a heterogeneous population by such electrodes. To illustrate, Figs. 16 and 17 show responses from heterogeneous populations produced by the two-pulse strategy first described in section II.D for coding latency breaks in the terminal region. Although the fields are obviously more complex than the fields from a uniform population (Fig. 9), it is also clear that ranges of stimulus parameters exist over which a single, long-latency "tail" can be produced at the apical end of the response fields and a single, short-latency region can be produced at the basal end. Differences in the response fields between heterogeneous and uniform populations include (a) a "smearing" or greater distribution of locations of the apical tails for the heterogeneous

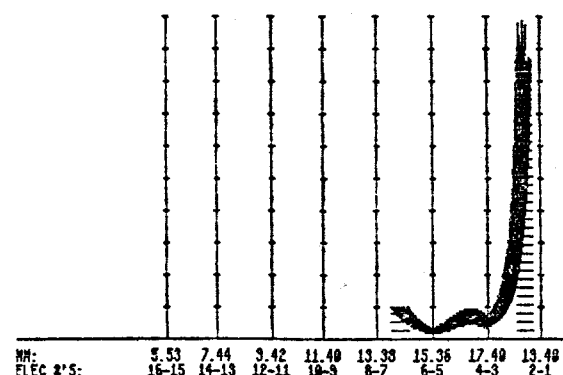
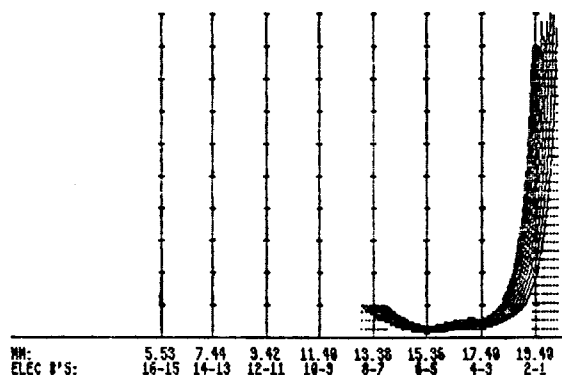
One site of excitation

Stimuli

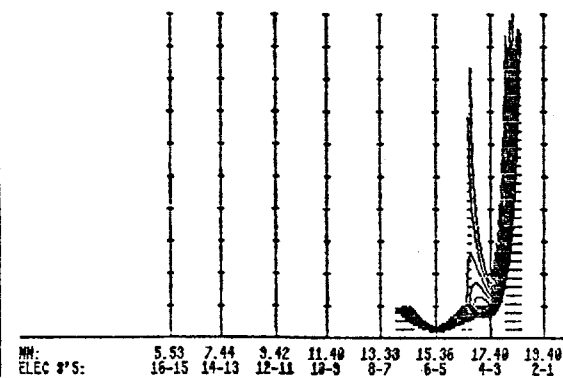
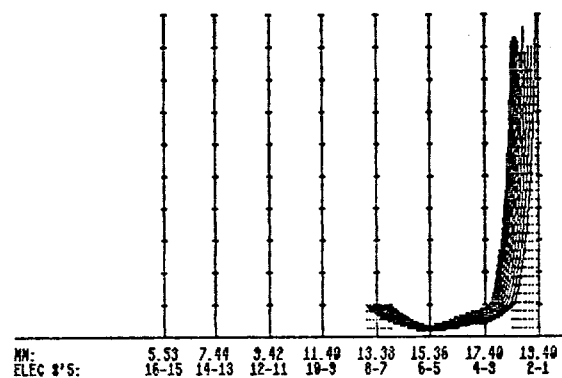
$\lambda = 1.4$ mm

$\lambda = 0.87$ mm

6-5: 500 μ A,
100 μ sec
4-3: 200 μ A,
1000 μ sec



6-5: 500 μ A,
100 μ sec
4-3: 100 μ A,
1000 μ sec



6-5: 300 μ A,
100 μ sec
4-3: 70 μ A,
1000 μ sec

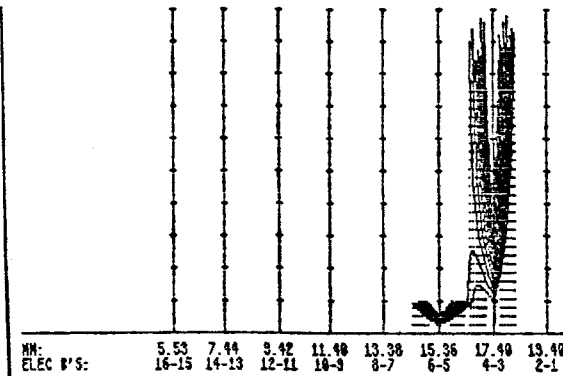
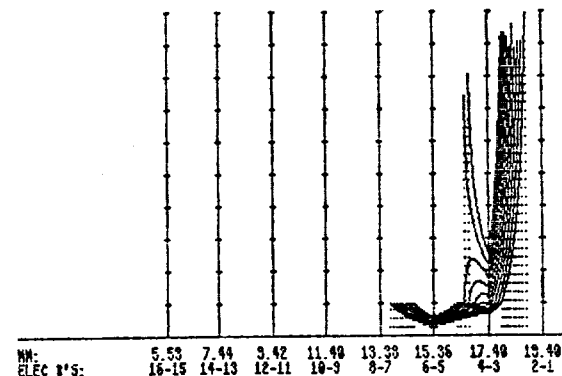


Fig. 16. Predicted latency fields for short-duration, high-intensity pulses delivered to electrode pair 6-5 in combination with long-duration, low-intensity pulses delivered to electrode pair 4-3. The space constant for the left column of panels is 1.4 mm, and the space constant for the right column of panels is 0.87 mm. The values of rheobase and chronaxie are presented in the caption of Fig. 11. The maximum latency for all panels in the present figure is 1000 μ sec. Note that control of latency fields is more difficult (but still possible) with a heterogeneous population of neurons than with single neurons, as in the simulations of Fig. 9.

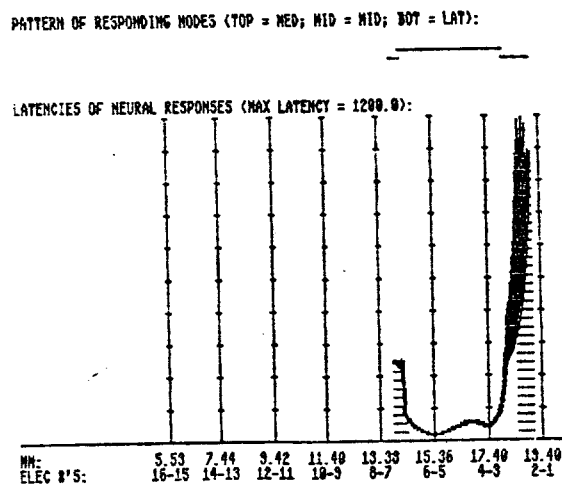
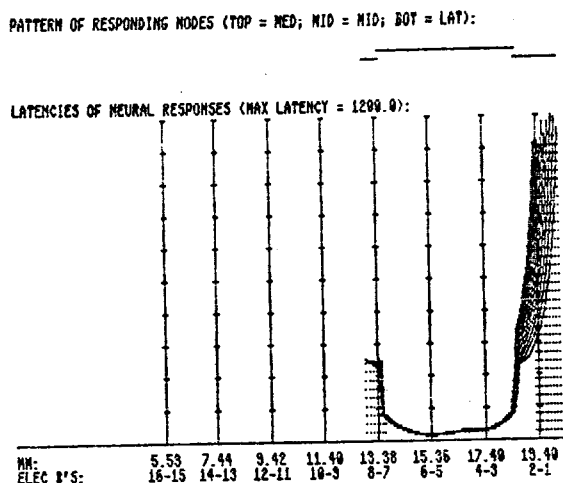
Two sites of excitation

Stimuli

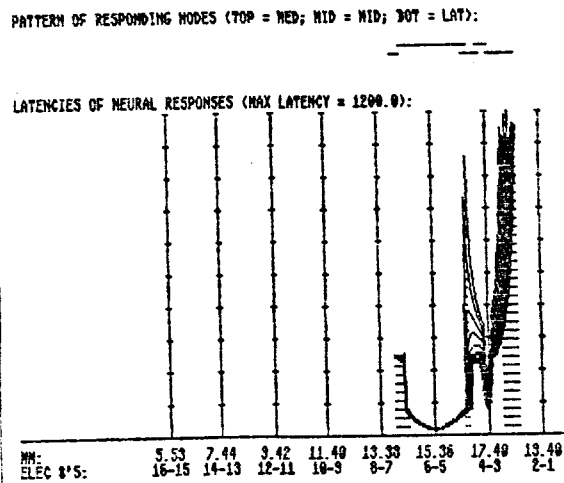
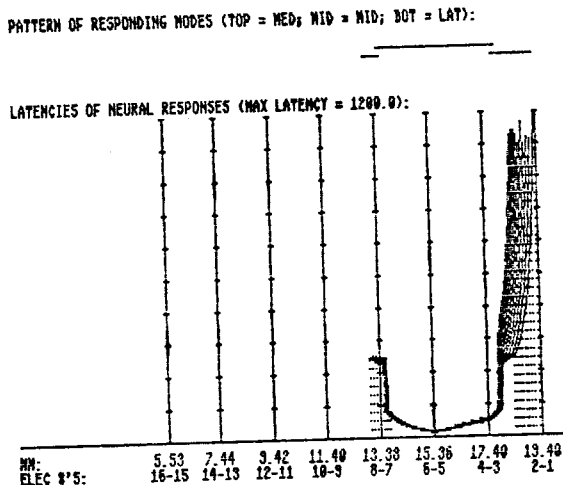
$\lambda = 1.4 \text{ mm}$

$\lambda = 0.87 \text{ mm}$

6-5: 500 μA ,
1000 μsec
4-3: 200 μA ,
1000 μsec



6-5: 500 μA ,
100 μsec
4-3: 100 μA ,
1000 μsec



6-5: 300 μA ,
100 μsec
4-3: 70 μA ,
1000 μsec

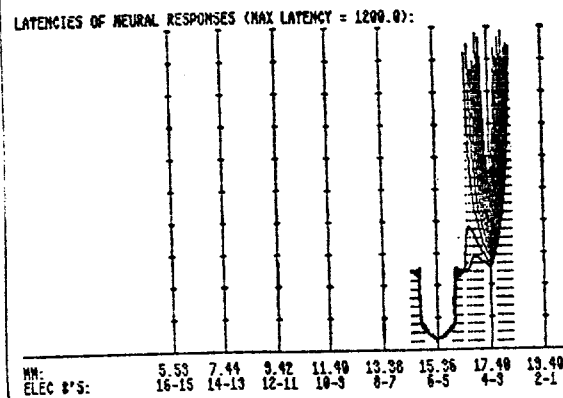
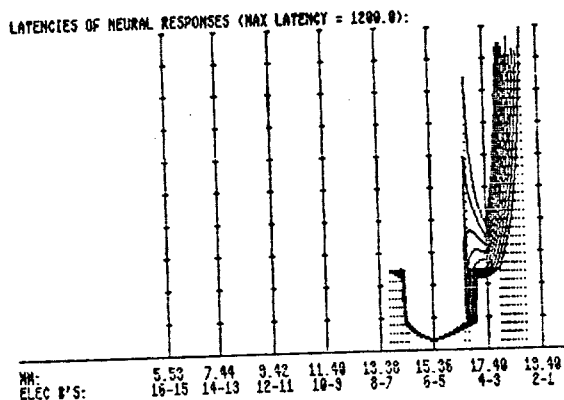


Fig. 17. (caption on next page)

Fig. 17. Predicted latency fields for the conditions of Fig. 16, except that the model neurons in the present figure are designed to simulate a reduction in "effective chronaxie" when stimulus intensity is raised 2-to-3 times above threshold (see caption of Fig. 15 for details). The maximum latency for all panels in the present figure is 1200 μ sec. Note that the latency fields in this figure are somewhat more complex over the basal electrode pair (6-5) than the corresponding fields in Fig. 16.

population; (b) a somewhat narrower range of stimulus parameters over which latency breaks can be coded for the heterogeneous population; and (c) the introduction of additional (but small) latency discontinuities in the response fields for heterogeneous populations where both dendritic and axonal sites of stimulation are modeled (Fig. 17). These differences might be expected to degrade but not destroy the representation of stimulus frequency by latency breaks beyond the apical electrode(s).

Because the curves of individual neurons are not tightly clustered in the response fields found for stimulation of heterogeneous populations with monopolar electrodes (Fig. 12), manipulation of latency profiles to code stimulus intensity and frequency is much more difficult with monopolar electrodes than with spatially-selective electrodes. That is, the dispersion in the response fields evoked by monopolar electrodes works against coding strategies that seek to control latency profiles over restricted segments of the cochlear partition. The previous remarks on basic effects of pulse parameters on neural response fields (section II.B), however, also apply to the present case of monopolar stimulation of heterogeneous populations of neurons. Finally, we note that the temporal channel interactions described in section II.E would also be found for such stimulation.

G. Remarks on dendritic versus axonal stimulation

A central problem in research on cochlear implants is to explain how good performance can be obtained in certain "star" patients with single-channel devices or with multichannel devices using monopolar electrode arrays. With either class of devices spatial selectivity of excitation is thought to be very poor or nonexistent. In the previous subsection we have outlined a way in which the spatial selectivity of multichannel monopolar stimulation might be sharper than previously thought (Fig. 13; Table 3). This would explain the ability of patients implanted with monopolar arrays to rank their electrodes according to location (see, e.g., Eddington et al., 1978). However, as outlined above, a rich population of surviving dendrites is probably required for the effect.

In this subsection we will mention another way in which dendritic activation might have a advantage over axonal stimulation. First, we note

that the ranges of anatomical features (such fiber diameter, nodal dimensions and inter-nodal lengths) are greater for the dendrites than for the axons of the auditory nerve (Lieberman and Oliver, 1984). These greater ranges undoubtedly produce greater ranges of neural response properties for intracochlear electrical stimulation. Indeed, the data and van den Honert and Stypulkowski (1984) show a much greater range and variability for chronaxies of neurons with intact dendrites than the range and variability for chronaxies of neurons whose dendrites are removed (in a laminectomy preparation). In addition, the range of rheobases is much greater in the intact population than in the dendrites-removed population. Selective activation of the dendrites is therefore likely to introduce a greater heterogeneity in neural responses than is axonal stimulation. A greater heterogeneity in the response fields may in turn allow for a higher temporal bandwidth of information to be represented in the ensemble response. That is, because not every neuron is stimulated on every cycle of a repetitive stimulus, different "subsets" of stimulated neurons can represent each succeeding cycle*. A requirement for this "time-shared" representation of high-frequency information is stochastic independence between neurons in the excitation field. A degree of independence is produced by the relative heterogeneity of anatomical and related response properties of the dendrites. Also, the greater and more-variable absolute and relatively-refractory periods of dendritic activation as opposed to axonal activation (Stypulkowski and van den Honert, 1984, Figs. 2 and 5) would tend to impart different discharge histories among stimulated neurons. The different discharge histories could further improve the ability of the nerve to convey temporal information. Specifically, the burden of information transfer is shared between previously-stimulated neurons still in their refractory periods and fully-recovered neurons, now ready for stimulation on the present stimulus cycle.

*This, of course, is a statement of Wever's volley theory of pitch perception in which frequencies as high as 3 to 4 kHz can be represented in the ensemble response even though individual auditory neurons can only respond up to about 200 spikes/s.

Another factor which may favor dendritic activation is the fact that the relative level of membrane noise ($1/f$ noise) increases as the diameter of a myelinated neuron decreases (Verveen, 1959 and 1962; Verveen and Dirksen, 1968; Mark White, personal communication). Effects of membrane noise will therefore be greater at the dendrites than at the axons. One manifestation of increased membrane noise would be increases in the variabilities of thresholds and latencies of single-unit responses to electrical stimuli. Such increases are clearly evident in comparisons of latency jitter and threshold variability between single units in the intact (with dendrites) and laminectomy (without dendrites) preparations of van den Honert and Stypulkowski (1984, Fig. 4 and Table 1). In addition, responses near threshold in the intact preparations of Hartmann *et al.* (1984a and b) exhibit much greater latency jitter than responses at higher stimulus levels. Inasmuch as dendritic activation occurs near threshold for intact preparations for the types of electrodes used, and inasmuch as axonal activation occurs at higher stimulus levels (2 or 3 times above threshold; see Stypulkowski and van den Honert, 1984, Figs. 1 and 7), the results of Hartmann *et al.* also support the notion of greater effects of membrane noise at the dendrites.

The effects of greater membrane noise, greater variability in neural response properties, and greater and more variable refractory periods for dendritic activation over axonal activation may act together to increase the temporal bandwidth of information that can be represented with an auditory prosthesis when the dendrites are selectively stimulated. In the previous subsection we showed that stimulation with the spatially-diffuse electric fields of monopolar electrodes is likely to restrict neural excitation to dendritic sites, while stimulation with spatially-selective electrodes is likely to excite axonal nodes at stimulus levels much above threshold. Therefore, a tradeoff between spatial selectivity and temporal bandwidth could exist for auditory prostheses. In the extreme case of a single-channel device excellent temporal bandwidth could overcome the deficits imposed by a lack of spatial selectivity. Indeed, such a tradeoff might explain the performance of "star" patients using the single-channel Hochmair device (Hochmair-Desoyer *et al.*, 1985). With this device a four-channel electrode array is inserted into the scala tympani. Then, when healing is complete, measures of threshold, dynamic range and temporal gap detection are obtained for all channels. The one channel that exhibits the best of

these measures is selected for stimulation with the output of a single-channel speech processor. Because all three measures are likely to be better for stimulation of neurons with surviving dendrites than for neurons without surviving dendrites, this procedure increases the probability of matching a somewhat-selective excitation field (produced by the Hochmair electrodes, see discussion in section II.A) with populations of neurons that have intact dendrites. This matching of stimulation fields to dendrites could be critical to the successes of the Hochmair device inasmuch as dendritic survival is patchy in many deaf ears (Hinojosa and Marion, 1983). For patients with poor dendritic survival, of course, no amount of matching would be expected to produce a good result. This last expectation is consistent with the high degree of variability in speech-recognition scores found among patients in the Vienna series.

H. Concluding remarks

Most of the results presented in this report were obtained with a simple ensemble model that couples an exponential-falloff model of electric field patterns with a mathematical description of strength-duration curves for intracochlear electrical stimulation. These results are consistent with the following observations:

1. A parabolic-like profile of latencies is found in the fields of neural responses evoked by stimulation with intracochlear electrodes;
2. The extent of the excitation field, and the shape of the latency profile, are not necessarily constant for stimulation with constant-charge pulses;
3. Fundamental attributes of the auditory stimulus, such as intensity and frequency, might be coded by appropriate manipulations in the latency profiles of evoked neural responses;

4. Severe interactions between channels can be produced by simultaneous stimulation of different electrodes (or electrode pairs) in a multichannel array;
5. Response fields found in a heterogeneous population of neurons are similar to the fields found for a uniform population for spatially-selective electrodes, but dissimilar in important ways for electrodes with large space constants;
6. Surprisingly, the "equivalent space constants" of the neural density profile found for monopolar stimulation can be much less than the space constants of the imposed electric field;
7. This may explain how patients implanted with monopolar arrays can rank their electrodes;
8. For patients with good nerve survival monopolar electrodes may preferentially excite dendritic nodes over the dynamic range of stimulation, while bipolar electrodes may excite dendritic nodes near threshold and axonal nodes thereafter;
9. It is likely that a higher bandwidth of temporal information can be represented to the central auditory system with dendritic activation than with axonal activation; and
10. Therefore a tradeoff between spatial selectivity and temporal bandwidth may exist for auditory prostheses.

In summary, then, our simple ensemble model appears to provide a powerful tool for demonstrating basic patterns of neural responses evoked by intracochlear electrical stimulation and for generating testable hypotheses of improved stimulus coding for cochlear implants. We will be evaluating the hypotheses implicit in points 3, 7 and 10 above in tests with future implant patients. In addition, we plan to develop and apply the more-sophisticated ensemble models outlined in the introduction to section II. As mentioned there, these models should allow us to elucidate details in the

responses fields not evident in the predictions of ensemble model 1.
Results of these future studies will be reported as they become available.

III. Plans for the Next Quarter

Our first implant patient at Duke Medical Center is scheduled for surgery on 10/24/85. This operation will be the first of two: the initial operation to insert the intracochlear electrode array and install a percutaneous cable for direct access to the electrodes; and the second operation to remove the percutaneous cable and install the receiver disk for the UCSF/Storz transcutaneous transmission system. We expect that tests with the percutaneous cable will continue for 1-to-2 months after the first operation. Work in the next quarter will be devoted to preparation for, and subsequent conduct of, these tests. Follow-up tests with the transcutaneous transmission system will be performed on an infrequent basis after the second operation. Initial results from the percutaneous-testing phase will be presented in our next quarterly report.

IV. Acknowledgement

The work presented in this report is a first synthesis of many ideas that arose in enlightening discussions with colleagues. We are therefore delighted to acknowledge the important contributions made by M.W. White, M.M. Merzenich, F.T. Hambrecht, G.E. Loeb and R.V. Shannon.

V. References

- Allen, J.B., Magnitude and phase-frequency response to single tones in the auditory nerve, J. Acoust. Soc. Am., 73 (1983) 2071-2092.
- Black, R.C. and Clark, G.M., Differential electrical stimulation of the auditory nerve, J. Acoust. Soc. Am., 67 (1980) 868-874.
- Brismar, T., Potential clamp analysis of membrane currents in rat myelinated nerve fibers, J. Physiol., 298 (1980) 171-184.
- Chiu, S.Y., Ritchie, J.M., Rogart, R.B. and Stagg, D., A quantitative description of membrane currents in rabbit myelinated nerve, J. Physiol., 292 (1979) 149-166.
- Dobie, R.A. and Dillier, N., Some aspects of temporal coding for single-channel electrical stimulation of the cochlea, Hearing Res., 18 (1985) 41-55.
- Eddington, D.K., Dobelle, W.H., Brackmann, D.E., Mladejovsky, M.G. and Parkin, J.L., Auditory prosthesis research with multiple channel intracochlear stimulation in man, Ann. Otol. Rhinol. Laryngol., 87, Suppl. 53 (1978) 1-39.
- Hartmann, R., Topp, G. and Klinke, R., Electrical stimulation of the cat cochlea--Discharge pattern of single auditory fibres, Adv. Audiol., 1 (1984a) 18-29.
- Hartmann, R., Topp, G. and Klinke, R., Discharge patterns of cat primary auditory fibers with electrical stimulation of the cochlea, Hearing Res., 13 (1984) 47-62.
- Hinojosa, R. and Marion, M., Histopathology of profound sensorineural deafness, Ann. N.Y. Acad. Sci., 405 (1983) 459-484.

- Hochmair-Desoyer, I.G. and Hochmair, E.S., An eight channel scala tympani electrode for auditory prostheses, IEEE Trans. on Biomedical Engineering, BME-27 (1980) 44-50.
- Hochmair-Desoyer, I.J., Hochmair, E.S. and Stiglbrunner, H.K., Psychoacoustic temporal processing and speech understanding in cochlear implant patients. In R.A. Schindler and M.M. Merzenich (Eds.), Cochlaer Implants, Raven Press, New York, 1985, pp. 291-304.
- Kim, D.O., Molnar, C.E. and Matthews, J.W., Cochlear mechanics: Nonlinear behavior in two-tone responses as reflected in cochlear-nerve-fiber responses and in ear-canal sound pressure, J. Acoust. Soc. Am., 67 (1980) 1704-1721.
- Lieberman, M.C. and Oliver, M.E., Morphometry of intracellularly labeled neurons of the auditory nerve: Correlations with functional properties, J. Comp. Neurol., 223 (1984) 163-176.
- Loeb, G.E., White, M.W. and Jenkins, W.M., Biophysical considerations in electrical stimulation of the auditory nervous system, Ann. N. Y. Acad. Sci., 405 (1983) 123-136.
- Loeb, G.E., White, M.W. and Merzenich, M.M., Spatial cross-correlation: A proposed mechanism for acoustic pitch perception, Biol. Cybernetics, 47 (1983) 149-163.
- McNeal, D.R., Analysis of a model for excitation of myelinated nerve, IEEE Trans. BME, 23 (1976) 329-337.
- McNeal, D.R. and Teicher, D.A., Effect of electrode placement on threshold and initial site of excitation of a myelinated nerve fiber. In F.T. Hambrecht and J.B. Reswick (Eds.), Functional Electrical Stimulation: Applications in Neural Prostheses, New York, Marcel Dekker (1977), pp. 405-412.

- Merzenich, M.M. and White, M., Cochlear implants: The interface problem. In F.T. Hambrecht and J.B. Reswick (Eds.), Functional Electrical Stimulation: Applications in Neural Protheses, New York, Marcel Dekker (1977), pp. 321-340.
- Muller, C.G., Comparison of percepts found with cochlear implant devices, Ann. N.Y. Acad. Sci., 405 (1983) 412-420.
- O'Leary, S.J., Black, R.C., and Clark, G.M., Current distributions in the cat cochlea: A modelling and electrophysiological study, Hearing Res., 18 (1985) 273-281.
- Pfingst, B.E., Evans, M., Garrido, Y. and Rush, N., Frequency difference limens for electrical stimulation of the deafened inner ear. In ARO Abstracts, 8th Midwinter Research Conference, 1985, p. 107.
- Ranck, J.B., Jr., Which elements are excited in electrical stimulation of mammalian central nervous system: A review, Brain Res., 98 (1975) 417-440.
- Sachs, M.B., Speech encoding in the auditory nerve. In C. Berlin (Ed.), Hearing Science, College-Hill Press, San Diego (1984), pp. 263-307.
- Shamma, S.A., Speech processing in the auditory system. I: The representation of speech sounds in the responses of the auditory nerve, J. Acoust. Soc. Am., 78 (1985a) 1612-1621.
- Shamma, S.A., Speech processing in the auditory system. II: Lateral inhibition and central processing of speech evoked activity in the auditory nerve, J. Acoust. Soc. Am., 78 (1985b) 1622-1632.
- Shannon, R.V., Multichannel electrical stimulation of the auditory nerve in man. I. Basic Psychophysics, Hearing Res., 11 (1983) 157-189.

- Simmons, F.B., Walker, M.G., Mathews, R.G. and White, R.L., Percepts and discrimination by auditory nerve stimulation: A summary of results and some proposals for nerve viability evaluation. In D.L. McPherson and M.S. Davis (Eds.), Advances in Prosthetic Devices for the Deaf: A Technical Workshop, National Technical Institute for the Deaf, Rochester Institute of Technology, Rochester, N.Y., 1979, pp. 271-274.
- Snyder, R.L. and Schreiner, C.E., Forward masking of the auditory nerve neurophonic (ANN) and the frequency following response (FFR), Hearing Res., 20 (1985) 45-60.
- Stypulkowski, P.H. and van den Honert, C., Physiological properties of the electrically stimulated auditory nerve. I. Compound action potential recordings, Hearing Res., 14 (1984) 205-223.
- van den Honert, C. and Stypulkowski, P.H., Physiological properties of the electrically stimulated auditory nerve. II. Single fiber recordings, Hearing Res., 14 (1984) 225-243.
- van den Honert, C. and Stypulkowski, P., Spatial mapping of electrical excitation patterns within the cochlea derived from single fiber responses, Abstr. of the 8th ARO Meeting, p. 106, 1985.
- Verveen, A.A., On the fluctuation of threshold of the nerve fiber. In D.B. Tower and J.B. Shade (Eds.), Structure and Function of the Cerebral Cortex: Proceedings of the Second International Meeting of Neurobiologists, Amsterdam, 1959.
- Verveen, A.A., Fibre diameter and fluctuation in excitability, Acta Morphologica Neerlandico-Scandinavica, 5 (1962) 79-85.
- Verveen, A.A., Derksen, H.E., Fluctuation phenomena in nerve membrane, Proc. IEEE, 56 (1968) 906-916.

Appendix 1

Abstracts Prepared in the Present Quarter

1. BS Wilson and CC Finley, "Latency Fields in Electrically-Evoked Hearing," to be presented at the 9th ARO Meeting, 2/6/86;
2. CC Finley and BS Wilson, "Sampling of Electrical Fields by Myelinated Intracochlear Neurons," to be presented at the 9th ARO Meeting, 2/6/86;
3. CC Finley and BS Wilson, "Models of Neural Stimulation for Electrically Evoked Hearing," to be presented at the 38th ACEMB Meeting, 9/30-10/2/85;
4. BS Wilson and CC Finley, "Speech Processors for Auditory Prostheses," to be presented at the 8th IEEE-EMBS Meeting, 9/27-9/30/85; and
5. CC Finley and BS Wilson, "A Simple Finite-Difference Model of Field Patterns Produced by Bipolar Electrodes of the UCSF Array," to be presented at the 8th IEEE-EMBS Meeting, 9/27-9/30/85.

LATENCY FIELDS IN ELECTRICALLY-EVOKED HEARING.

*B.S. Wilson and C.C. Finley, Neuroscience Program Office, Research Triangle Institute, Research Triangle Park, N.C. 27709.

In this presentation we will describe models that predict the spatial and temporal patterns of neural responses produced by intracochlear electrical stimulation. The simplest of these models couples a mathematical description of the field patterns generated by intracochlear electrodes with a mathematical description of strength-duration curves for electrical stimulation. The mathematical description of the field patterns ranges in complexity from an exponential-falloff model to our spiral-plane, finite-difference model of the UCSF electrode array (8th ARO, p. 105, 1984); data for the strength-duration model are obtained from the measurements of Loeb et al. (NYAS, 405:123-136, 1983) and van den Honert and Stypulkowski (Hearing Res., 14:225-243, 1984). For the exponential-falloff description of the electric field patterns, a parabolic-like profile of latencies is predicted by the combined model for monophasic, rectangular pulses. That is, as distance from the stimulating electrode (or electrode pair) increases, the electric field falls off and neurons at these locations are stimulated further and further out along their strength-duration curves. Ultimately, the strength of the current field falls below threshold (for the duration of the pulse) and neurons at locations more distant than this point are not stimulated. Manipulations of pulse intensity and duration have large effects (even for constant charge) on the extent of the excitation field and on the synchronicity of discharge across this field. These effects are highly correlated with psychophysical measures of loudness and threshold. Finally, the patterns of neural responses predicted with the finite-difference model of the UCSF array are in general more complex than the patterns just described for the exponential-falloff model. In particular, large discontinuities in the latency fields are predicted for balanced biphasic pulses delivered to the offset radial pairs of the UCSF array. Possible perceptual correlates of these discontinuities and other features of the latency fields will be listed; and the latency fields predicted for electrically-evoked hearing will be compared with the latency fields found in normal hearing. In our concluding remarks, we will mention some ways in which the latency fields produced in electrically-evoked hearing might be made to approximate the latency fields of normal hearing.

SAMPLING OF ELECTRICAL FIELDS BY MYELINATED INTRACOCHLEAR NEURONS

*C.C. Finley and B.S. Wilson, Neuroscience Program Office, Research Triangle Institute, Research Triangle Park, N.C. 27709.

The response of a myelinated neuron to electrical stimulation within the cochlea depends upon both the profile of the electrical field outside the neuron and upon how the neuron samples or interacts with the field. The extracellular field pattern is largely determined by the geometries and placements of the electrodes within the cochlea and by the effects of differing impedances of various tissues within the cochlea. Sampling of the electrical field by a myelinated neuron occurs predominately at node locations. Polarizing currents crossing the nodal membranes determine the responses of each node to the external potential field. The magnitude of these currents is a function of the impedances of the nodal regions and the intranodal core resistances. For a large diameter fiber, intranodal core resistances are low compared to the high nodal impedances, so nodal impedances primarily determine the magnitude of the polarizing currents for a given extracellular field magnitude. Consequently, current magnitudes at these nodes are largely independent of the conditions at adjacent nodes and are therefore more sensitive to the absolute magnitude of the extracellular field at each node. For a small diameter fiber, intranodal core resistances are higher and approach the magnitude of the nodal impedances. The small diameter fiber would therefore be more sensitive to the relative potential levels between adjacent nodes and thus would respond to regions of high gradients as opposed to absolute magnitude of the extracellular electrical field. Type 1 ganglion cells in the cat have been described as having small diameter dendrites with relatively-large diameter central axons (Kiang et al., Science 217:175-177, 1982). These anatomical variations raise the possibility that type 1 ganglion cells sample electrical fields in different manners at the dendrites and central axons. This possibility is also of significance in designing bipolar electrodes that would be effective in situations of both good and poor dendrite survival.

In this presentation we will describe evaluations of the relative significance of absolute magnitude versus potential gradients of extracellular fields on modelled type 1 ganglion cells. The cells are modelled using our integrated field-neuron model of electrical stimulation (8th ARO, p. 105, 1984). Discussion will include the relative influences of monopolar and bipolar electrode configurations and will conclude with comments on how these results pertain to improved electrode design.

C.C. Finley and B.S. Wilson

Design of advanced speech processors for multichannel auditory prostheses requires detailed knowledge of the mechanisms of electrical neural stimulation occurring within the cochlea. Such knowledge will afford the opportunity to optimize the coding of speech information by gaining precise control over the firing patterns evoked among fibers of the VIIIth nerve. Many factors are known to contribute to the overall characteristics of the "electrical-to-neural transformer" that links stimuli delivered to intracochlear electrodes to discharge patterns in the auditory nerve. These factors include the physical locations, dimensions and electrical characteristics of the electrodes, as well as, the physiological integrity and survival patterns of the remaining neural elements. In addition, to achieve successful encoding of speech on the VIIIth nerve by electrical stimulation, it is probably necessary to control the temporal and spatial profiles of neural discharge around each electrode or electrode pair while avoiding and/or exploiting field interactions between the electrodes. To evaluate the relative significance of each of these contributing factors, we have developed a series of computer-based models which describe the events of neurostimulation within the cochlea.

The first model describes the electrical field patterns within the cochlea, as a consequence of stimulation by electrodes within scala tympani. The objective of this model is to provide estimates of the profiles of potentials along the loci of surviving neural elements. These potentials are calculated by an iterative, two-dimensional, finite difference model of a cochlear cross section, which includes a pair of electrodes in the scala tympani. Grid points in the model are 20 microns apart and resistivities linking the grid points are defined according to published values for resistivities of tissues and fluids appearing in the cross section. The bipolar electrodes are defined as equipotential conductors mounted in an insulating carrier medium. Fixed voltages are assigned to each electrode and the resultant field patterns are computed by iteration for the entire cross section. Potential levels at points along the loci of the VIIIth nerve elements are extracted from the final field calculation. A second version of this model, containing the spiral of the cochlea, compressed into two dimensions, is used to estimate the interaction and crosstalk at a single neural element for stimulation of two or more electrode channels. Both models provide field pattern estimates that correlate well with published data from animal experiments.

A second model is a lumped-element description of an electrically-stimulated, myelinated neuron. Stimulus inputs for the model are the potential profiles calculated in the field potential models described above. This model is a modification of McNeal's axon model (IEEE Trans. BME 23: 329-337, 1976) of resistively-linked Frankenhauser-Huxley nodes. The modified model includes myelinated axon cable properties and uses mammalian node of Ranvier characteristics instead of the characteristics for Frankenhauser-Huxley frog nodes. Eighteen active nodes are included, each separated by ten myelinated segments. One section includes characteristics of a cell body, resembling the bipolar cells of the cochlea. A system of simultaneous, nonlinear differential equations is solved iteratively to calculate the model's response to any arbitrary stimulus waveform, applied as a voltage profile along the entire length of the axon. The neuron model, in conjunction with the field potential models, constitutes an integrated model of single fiber behavior in the electrically-stimulated cochlea.

However, speech encoding in the cochlea requires successful temporal control of an ensemble of neurons spatially distributed along the cochlear partition. A third model has been developed to describe ensemble responses of multiple neurons to stimulation by multiple electrodes. This model allows manipulation of field patterns and channel configurations of the electrodes, along with response characteristics and survival patterns of the neural elements. "Latency profiles" are calculated which show timing of neural firing as a function of both the location of the element along the cochlea and the stimuli and electrode channel configurations used. Initial studies indicate the occurrence of abrupt discontinuities in response fields as a consequence of electrode polarity and neural survival. These response discontinuities complicate the design of speech processors which seek to replicate firing patterns of the normal cochlea in response to speech stimulation.

(Supported by NIH Contract N01-NS-2356, "Speech Processors for Auditory Prostheses.")

Research Triangle Institute
Neuroscience Program Office
P.O. Box 12194
Research Triangle Park, N.C. 27709

(KEMAR). Using a pseudorandom noise input, the phase characteristic of the transfer function at a high volume control setting was obtained with an FFT-based spectrum analyzer as well as the group delay through the hearing aid *in situ*. These measurements were repeated with a phase compensator designed to improve the linearity of the phase characteristic. The effect of the phase compensator was to flatten the group delay through the hearing aid which may result in improved speech perception for hearing impaired persons.

Speech Processors for Auditory Prostheses

BLAKE S. WILSON AND CHARLES C. FINLEY

In this presentation, we will describe strategies for coding speech signals for auditory prostheses. Two problems will be considered: 1) the "classic" problem of extracting parameters from speech that are essential for intelligibility, and 2) the problem of transforming these parameters into electrical stimuli that will produce patterns of neural activity that are perceived as intelligible speech.

Speech Processing for Cochlear Implants

E. L. V. WALLEMBERG, I. J. HOCHMAIR-DESOYER, AND
E. S. HOCHMAIR

Open-list sentence understanding without lipreading can be achieved by single-channel analog broad-band electrical stimulation by 75 percent of the postlingually deafened patients equipped with a Vienna cochlear prosthesis. Based on the analysis of vowel identification tasks, alternate speech coding strategies using feature extraction have been developed and evaluated.

Session C13—Cochlear Prostheses

Implications of Speech Encoding in the Normal Cochlea for a Cochlear Prosthesis

BEN M. CLOPTON

In addition to established analysis and transduction processes in the normal cochlea, significant nonlinearities and, possibly, extracellular electrical currents influence activity in the auditory nerve. Enhancement of specific features in sound waveforms, especially speech, occurs. These processes imply strategies for electrically encoding speech information for a cochlear prosthesis.

Current Spreading and Current Deconvolution in Scala Tympani Prostheses

DIRK VON COMPERNOLLE AND ROBERT L. WHITE

Multielectrode cochlear arrays have the potential to create, at the neurons, a current density representing the complex energy density spectrum of speech. For present devices, the desired current pattern is placed on the electrodes and degraded by current spreading to a blurred representation at the neurons. If the current spreading function is known, however, so is its inverse; and it is possible, using "current deconvolution," to compute the current pattern required at the electrodes to produce the desired pattern at the neurons. This paper will deal with the potential and the limitations of current deconvolution techniques as applied to scala tympani cochlear prostheses.

A Simple Finite-Difference Model of Field Patterns Produced by Bipolar Electrodes of the UCSF Array

C. C. FINLEY AND B. S. WILSON

A finite-difference model of field patterns produced by the UCSF multichannel bipolar electrode array is presented. The model describes the array as a spiral, compressed into a two-dimensional, homogeneous plane. Potential levels along radially directed dendrites of spiral ganglion cells are described. Comparisons between of measured animal data and model predictions are presented. Implications for channel interaction phenomena are discussed.

Mixed Boundary Value Problems in the Implanted Cochlea

J. T. RUBINSTEIN, M. SOMA AND F. A. SPELMAN

This paper describes a three-dimensional analytical model of a finite-sized, cylindrical, segmented electrode array. The assumptions made are that the fields will be calculated at a distance much smaller than the length of the carrier, the carrier is a perfect insulator, and the electrodes are perfect conductors.

A Peak-Counting Model for Single-Electrode Cochlear Stimulation

LES ATLAS

A peak-counting model has been developed to predict the pitch and timbre perception for complex single-electrode electrical stimulation waveforms. This model has been studied for the case of amplitude modulated biphasic pulses and for more complex analog waveforms. The model has also been utilized to suggest speech processing algorithms.

Behavioral Responses to Intracochlear Electrical Stimulation: Possible Peripheral-Nerve Mechanisms

MARK WHITE

The rate at which neural activity increases with stimulus intensity is a function of fiber diameter. In addition, the intraaxonal resistance between nodes of Ranvier is a strong function of fiber diameter. These two primary factors may cause cochlear fibers of different diameter to be selectively excited depending on the stimulus level, the stimulus waveform, and distribution of surviving nerve.

Session D12—Electrical Control of Arrhythmias

Computer Algorithms for Tachycardia Detection in Antitachycardia Pacing

THOMAS E. BUMP

We have developed sensitive and specific decision rules for tachycardia identification which use rate in both chambers and degree of atrioventricular association to diagnose among tachycardias which do not have 1:1 atrioventricular relationship. Our technique delivers an atrial extrastimulus to differentiate sinus tachycardia from other